1966

Effects of electron correlation in X-ray diffraction and an electron diffraction study of XeF6

Robert Michael Gavin Jr.
Iowa State University

66–10,419

GAVIN, Jr., Robert Michael, 1940–

EFFECTS OF ELECTRON CORRELATION IN X–RAY DIFFRACTION AND AN ELECTRON DIFFRACTION STUDY OF XeF_6.

Iowa State University of Science and Technology
Ph.D., 1966
Chemistry, physical

University Microfilms, Inc., Ann Arbor, Michigan

EFFECTS OF ELECTRON CORRELATION IN X-RAY DIFFRACTION AND AN ELECTRON DIFFRACTION STUDY OF XeF_6

by

Robert Michael Gavin, Jr.

A Dissertation Submitted to the
Graduate Faculty in Partial Fulfillment of
The Requirements for the Degree of
DOCTOR OF PHILOSOPHY

Major Subject: Physical Chemistry

Approved:

Signature was redacted for privacy.

In Charge of Major Work

Signature was redacted for privacy.

Head of Major Department

Signature was redacted for privacy.

Dean of Graduate College

Iowa State University
Of Science and Technology
Ames, Iowa

1966

TABLE OF CONTENTS

INTRODUCTION

The purposes of this research were (a) to investigate the information derivable, in principle, from observed intensities of scattered x rays, (b) to investigate properties of atomic electron-electron radial distribution functions, and (c) to determine the geometry of the xenon hexafluoride molecule by use of electron diffraction.

Even though scattering of high energy x rays was discussed perceptively by Debye (1) in 1915, it was not until the advent of quantum mechanics that extensive theoretical and experimental studies were undertaken. In the late 1920's, Waller and Hartree (2) developed theoretical expressions for intensities observed in x-ray diffraction experiments based on the then recent assumptions of quantum mechanics, and Barrett (3), Herzog (4), and Wollan (5) performed experimental studies of noble-gas atoms.

In the Waller-Hartree development, emphasis was placed on the relationship of observed intensity to the density of electrons about the nucleus. As a consequence of this emphasis, early experimental work centered on determination of one-electron radial densities from observed total intensities (6, 7, 8).

The Waller-Hartree expressions were derived assuming a specific form for the atomic wavefunction. It is possible, however, to deduce expressions quite different from the Waller-Hartree expressions by assuming a general form for the wavefunction and modifying the method of integration. If this alternative procedure is used, it becomes apparent that the total observed intensity is directly related to a two-electron density function and only indirectly related to the density of electrons about the nucleus.

Some properties of these two-electron radial distribution functions are studied in the present investigation and electron-electron radial distributions are deduced from observed total intensities of x rays.

Xenon hexafluoride was first prepared in 1962 by a number of workers (9, 10, 11, 12). Its preparation followed the discovery of the lower fluorides of xenon, XeF_4 (13) and XeF_2 (14, 15, 16, 17, 18). Since the discovery of the xenon fluorides, analyses have definitively established the structure of XeF_2 as linear (19, 20) and XeF_4 as square planar (21, 22, 23, 24). Attempts to establish the structure of XeF_6, however, have not been conclusive (25, 26). In addition, a number of theoretical treatments have resulted in conflicting predictions about the molecular geometry (27, 28, 29, 30).

An electron diffraction study was undertaken to determine if the molecule possessed octahedral symmetry as suggested by several authors (28, 29, 30). The results of this study show that the symmetry is not O_h and suggest a slightly distorted octahedral model containing Xe-F bonds of differing length.

CORRELATION EFFECTS ON X-RAY DIFFRACTION INTENSITIES

Theoretical Expressions

Theoretical expressions for the intensity of x rays scattered by gas atoms were developed by Waller and Hartree (2). Important contributions to the theory had been made previously by Wentzel (31) and Klein (32). Simplification and evaluation of the expressions for certain atoms have been made by other authors (33, 34, 35).

A first order perturbation approximation was used by Waller and Hartree to describe the nonrelativistic N-electron problem. The frequency of the incident radiation was assumed to be large compared to the K absorption frequency of the atom and the distance from scattering center to the point of observation was assumed large compared to atomic distances. In addition, recoil effects in inelastic events were neglected.

The resulting expressions for the total intensity $I_{tot}(\phi)$ and the intensity $I_{elas}(\phi)$ elastically scattered by independent atoms initially in state k, are

$$I_{tot}(\phi) = I_{cl} \int \Psi_k^* \left| \sum_i \exp(i\bar{s}\cdot\bar{r}_i) \right|^2 \Psi_k \, d\tau \qquad (1)$$

and

$$I_{elas}(\phi) = I_{cl} \left| \int \Psi_k^* \sum_i \exp(i\bar{s}\cdot\bar{r}_i) \Psi_k \, d\tau \right|^2 \qquad (2)$$

where ϕ is the total angle of scattering (twice the Bragg angle), I_{cl} is the intensity scattered by a point electron as derived from classical theory (36), Ψ_k is the electronic wavefunction of the atom, $\bar{r}_i$ describes

the position of the i^{th} atomic electron, and $\bar{s}$ is a vector of magnitude $(4\pi/\lambda)(\sin \phi/2)$ and direction $(\bar{n}_o - \bar{n})$, where $\bar{n}_o$ and $\bar{n}$ are unit vectors in the incident and scattered directions, respectively.

For spherically symmetric atoms or an average over random orientations of aspherical atoms, Equation 2 reduces to

$$I_{elas}(\phi) = I_{cl} \left| F(s) \right|^2. \tag{3}$$

The atomic scattering factor F(s) is given by

$$F(s) = \int_o^\infty D(r) \ (\sin sr)/sr \ dr \tag{4}$$

where

$$D(r) = \sum_i \int \Psi_k^* \Psi_k \ d\tau \ /dr_i. \tag{5}$$

Elastically scattered intensity is, then, a one-electron property which depends on the radial distribution D(r) of electrons about nuclei.

Simplification of Equation 1 may be accomplished by at least two different procedures. In the procedure adopted by Waller and Hartree (2), it is assumed that Ψ_k can be described by an antisymmetric combination of products of one-electron orbitals of the form

$$\Psi_k = A(u_1(1)u_2(2) \ . \ . \ . \ u_N(N)) \tag{6}$$

where

$$\int u_i(k)u_j(k)\ dv_k = \delta_{ij} \tag{7}$$

and A is the antisymmetrization operator. If Equation 1 is rearranged to the expression

$$I_{tot}(\phi) = I_{cl}\int \Psi_k^* \sum_i \sum_j \exp(i\bar{s}.\bar{r}_i)\exp(-i\bar{s}.\bar{r}_j)\ \Psi_k\ d\tau\ , \tag{8}$$

integration over all volume elements except dv_i and dv_j yields

$$I_{tot}(\phi) = I_{cl}[\ \sum_i \sum_j{}' (ii|jj) - (ij|ji) + N\ ] \tag{9}$$

where the prime denotes summation over all terms except for i=j and

$$(kl|mn) = \int u_k^*(i)u_m^*(j)\ \exp(i\bar{s}.(\bar{r}_i-\bar{r}_j))\ u_l(i)u_n(j)\ dv_i dv_j. \tag{10}$$

Functions of the form (kl|mn) may be expressed as products $f_{kl}f_{mn}^*$, with

$$f_{kl} = \int u_k^*(i)\ \exp(i\bar{s}.\bar{r}_i)\ u_l(i)\ dv_i,$$

so that Equation 8 has the form

$$I_{tot} = I_{cl}\ [\left|\sum_i^N f_{ii}\right|^2 - \sum_i^N f_{ii}^* f_{ii} - \sum_i^N \sum_j^N{}' f_{ij}\ f_{ji}^* + N\ ]. \tag{11}$$

The first term in Equation 11 is the elastic intensity defined by

Equation 3. The remaining terms are referred to as the inelastic intensity terms S(s), where

$$S(s) = N - \sum_i f_{ii}^* f_{ii} - \sum_i \sum_j{}' f_{ij} f_{ji}^* . \qquad (12)$$

The resulting formula for the total intensity is, then,

$$I_{tot} = I_{cl}[\,|F(s)|^2 + S(s)\,]. \qquad (13)$$

Equation 13 is the expression presented by Waller and Hartree (2) and that given in most standard reference books on the scattering of high energy x rays by gas atoms (37, 38).

An alternative procedure for integration of Equation 1 is possible and the resulting expression demonstrates an interesting property of I_{tot} which is not apparent in the above formulation. The first step is to recast Equation 1 into the form

$$I_{tot} = I_{cl} \sum_i \sum_j \int \Psi_k^* \exp(i\bar{s}\cdot\bar{r}_{ij})\, \Psi_k \, d\tau \qquad (14)$$

in which $\bar{r}_{ij} = (\bar{r}_i - \bar{r}_j)$. In this form it is evident that I_{tot} is a two-electron property related to the operator $\exp(i\bar{s}\cdot\bar{r}_{ij})$. The N-electron wavefunction depends on 3N spatial coordinates which may be conveniently taken as the components of the set $\bar{r}_1, \bar{r}_2, \ldots, \bar{r}_i, \bar{r}_{ij}, \bar{r}_k, \ldots, \bar{r}_N$ rather than the components of the set $\bar{r}_1, \bar{r}_2, \ldots, \bar{r}_i, \bar{r}_j, \bar{r}_k, \ldots, \bar{r}_N$. For spherically symmetric systems, integration over all coordinates except r_{ij} simplifies Equation 14 to

$$I_{tot} = I_{cl} \sum_{i}^{N} \sum_{j}^{N} \int_{o}^{\infty} P(r_{ij}) \, (\sin sr_{ij})/sr_{ij} \, dr_{ij} \tag{15}$$

where $P(r_{ij})$ is the radial distribution function of electron i with respect to electron j and is defined by

$$P(r_{ij}) = \int \Psi_k^* \Psi_k \, d\tau \, / dr_{ij}.$$

It should be noted that in this development no restrictions on the form of Ψ_k have been assumed. Any type of wavefunction, either correlated or uncorrelated, may be employed.

It is convenient to define a total electron-electron distribution function

$$P(r) = \sum_{i} \sum_{j \neq i}{}' P(r_{ij}) = \sum_{i} \sum_{j} P(r_{ij}) - N \, \delta(r) \tag{16}$$

which is analogous to the total electron-nuclear distribution function D(r). The $\delta(r)$ denotes a Dirac delta function. Equation 15 can then be expressed as

$$I_{tot} = I_{cl} \, [\int_{o}^{\infty} P(r) \, (\sin sr)/sr \, dr + N \,]. \tag{17}$$

Therefore, the total scattered intensity I_{tot} is a two-electron property which depends on the radial distribution P(r) of electrons about other electrons.

The electron-nuclear radial distribution D(r) and the electron-

electron radial distribution P(r) are related to elastic and total intensities, respectively, by Fourier sine integrals, as seen in Equations 4 and 17. Experimental radial distribution functions may be deduced from experimental intensity measurements by taking the appropriate Fourier sine transforms, or

$$D(r) = (2/\pi) \int_0^\infty sr\, F(s)\, (\sin sr)\, ds \tag{18}$$

and

$$P(r) = (2/\pi) \int_0^\infty sr\, (I_{tot}/I_{cl} - N)\, (\sin sr)\, ds. \tag{19}$$

The lack of experimental data to s of infinity may be handled by a procedure of the sort suggested by Hauptman and Karle (39). An experimental differentiation between elastic and total intensity is rarely carried out but it can be done, in principle, and has actually been accomplished in practice by Compton (40), at least for larger scattering angles.

Several experimental determinations of D(r) have been reported in which electron-nuclear distributions were deduced from total intensities (5, 7, 8, 41). In these determinations corrections for inelastic scattering were made using calculations from approximate wavefunctions. The natural information to be derived from total intensities, namely the electron-electron distribution function P(r), appears not to have been calculated. Inelastic corrections become smaller relative to the total intensity as the atomic number increases. For light atoms, however, the inelastic corrections in the most important angular range are comparable

to the elastic intensities. Consequently, the use of approximate wave-functions in the deduction of D(r) not only begs the question, logically, but also may lead to serious error. Moreover, since D(r) is a one-electron density function which is relatively simple to derive theoretically and since P(r) is a two-electron density function which is difficult to calculate, it would seem to be not only more rigorous but also more interesting to seek an experimental measure of P(r) rather than D(r) from I_{tot}.

The Hamiltonian operator for an atom may be taken, for the present purposes, as

$$H = \sum_i T_i + \sum_i V_{ni} + \sum_i \sum_{j>i} V_{ij} \tag{20}$$

where T_i and V_{ni} represent kinetic energy and electron-nuclear potential energy operators and where the V_{ij} operators represent the electron-electron repulsions. The distribution functions discussed in the preceding paragraphs characterize the electronic behavior sufficiently to establish the electronic energy completely. The average potential energies are

$$\overline{V}_{ne} = \sum_i \overline{V}_{ni} = -Z \int_o^\infty D(r)/r \ dr \tag{21}$$

and

$$\overline{V}_{ee} = \sum_i \sum_{j>i} \overline{V}_{ij} = (1/2) \int_o^\infty P(r)/r \ dr. \tag{22}$$

The total energy can be derived from the mean potential energy by use

of the virial theorem

$$E = (1/2)\ (\ \overline{V}_{ne} + \overline{V}_{ee}\ ). \tag{23}$$

Energies derived in this manner may not be comparable in accuracy to spectroscopic energies but do offer the possibility of obtaining the electron-electron and electron-nuclear contributions separately, which spectroscopic methods do not.

Theoretical Calculations

Electron-electron distribution functions

The distribution P(r) of electrons relative to other electrons in the atom is an important two-electron property which has received little attention in the literature (42, 43, 44, 45). Since by Equation 17 the total scattered intensity of x rays is directly dependent on this property, an investigation of these distributions seems to be in order.

The simplest electronic state which illustrates the two-electron aspects of P(r) is the $1s^2\ {}^1S$ state, one for which quite accurate wavefunctions are available. We shall be concerned with wavefunctions for these helium-like systems of the form

$$\Psi(\overline{r}_1, \overline{r}_2) = \phi(r_1)\ \phi(r_2)\ X(r_{12}) \tag{24}$$

in terms of which P(r) can be expressed as (42)

$$P(r_{12}) = 8\pi^2 r_{12} |X(r_{12})|^2 \int_0^\infty r_1\ dr_1 \int_{|r_{12}-r_1|}^{|r_{12}+r_1|} r_2 |\phi(r_1)\ \phi(r_2)|^2\ dr_2 \tag{25}$$

and D(r) as

$$D(r_1) = 8\pi^2 r_1 |\phi(r_1)|^2 \int_0^\infty r_2 |\phi(r_2)|^2 \, dr_2 \int_{|r_2-r_1|}^{(r_2+r_1)} r_{12} |X(r_{12})|^2 \, dr_{12}. \quad (26)$$

It is of interest to compare the behavior of D(r) and P(r) calculated according to a correlationless analytical Hartree-Fock (HF) wavefunction (46) and according to a correlated wavefunction of Roothaan and Weiss (47) which accounts for 92 percent of the correlation energy. Such a comparison for the ground state of the helium atom is made in Figure 1. Only one D(r) function was plotted in Figure 1 since the D(r) functions calculated from the two wavefunctions were indistinguishable from each other on the scale of the plot.

As discussed by several authors (48, 49, 50, 51), the Hartree-Fock results are considerably more accurate for the one-electron density than for the two-electron density. For this reason it is not surprising that the two D(r) functions are almost identical.

Calculations of D(r) and P(r) for helium-like systems with nuclear charges of 3, 4, 6, and 8 based on the correlated analytical wavefunctions of Roothaan and Weiss (47) and the analytical Hartree-Fock wavefunctions of Roothaan, Sachs, and Weiss (46) were carried out using the expressions of Equations 25 and 26. A comparison of these results permits an assessment of $\Delta P(r_{12})$, where

$$\Delta P(r_{12}) = P(r_{12})_{corr} - P(r_{12})_{HF},$$

the shift in $P(r_{12})$ due to correlated motions of electrons, for $1s^2\ {}^1S$

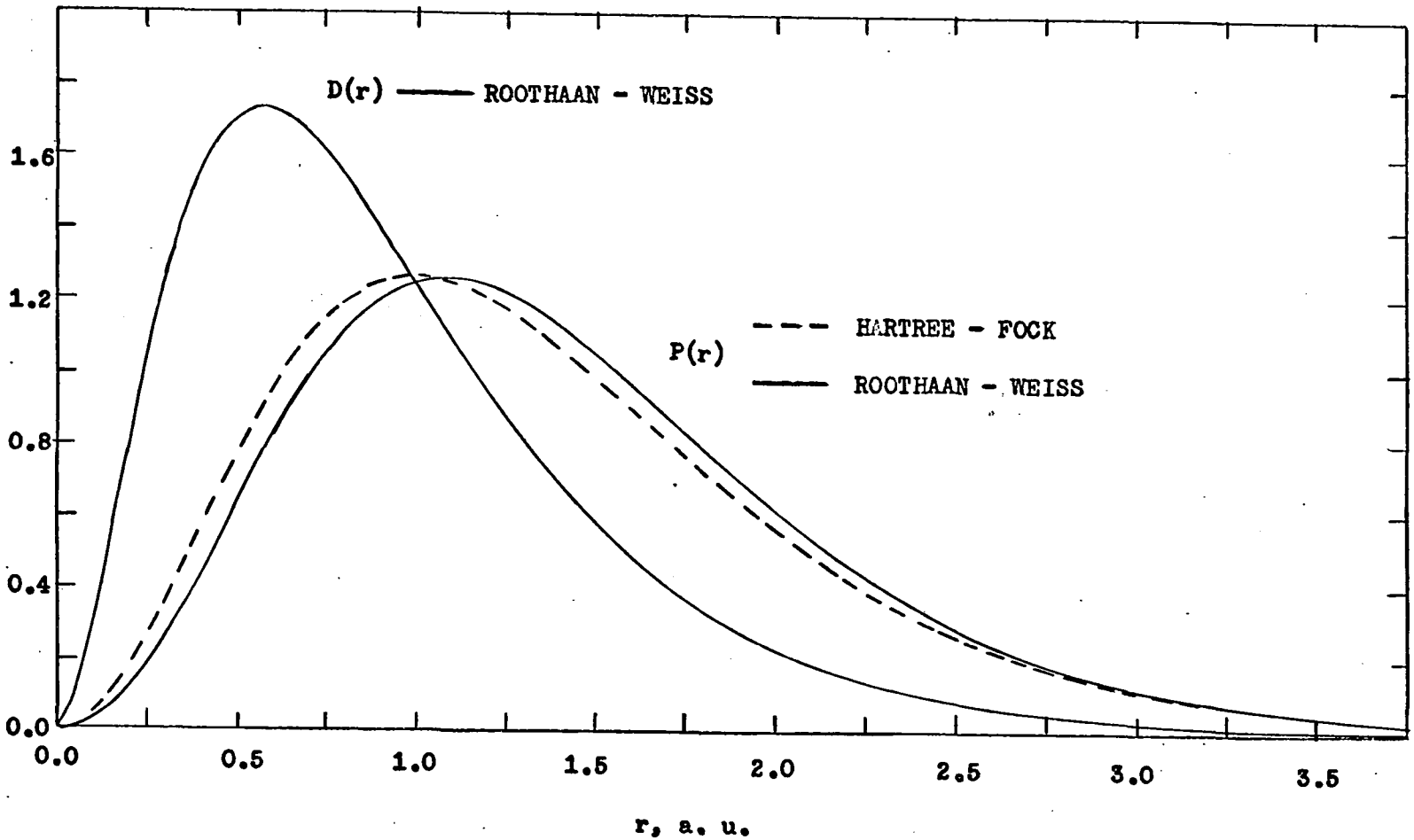

Fig. 1. Calculated electron-nuclear D(r) and electron-electron P(r) radial distribution functions for helium. The enhanced electron avoidance implicit in the Roothaan-Weiss wavefunction in comparison with the Hartree-Fock wavefunction is clearly evident.

electronic states with various nuclear charges.

The pair distribution functions $P(r_{12})$ calculated from the correlated wavefunctions are shown in Figure 2. Plotted in Figure 3 are the "Coulomb hole" functions $\Delta P(r_{12})$.

The $1s^2\ ^1S$ electronic states are, however, the simplest systems which may be studied. In order to obtain information from more complex systems, D(r) and P(r) distributions were calculated for the ground electronic state of the beryllium atom. Analytical Hartree-Fock wavefunctions of Roothaan, Sachs, and Weiss (46) and a configuration-interaction (CI) wavefunction of Boys (52) which accounts for 50 percent of the correlation energy were employed. A comparison of results permits an assessment of the shift in $P(r_{ij})$ due to electron correlation in a system with electron pairs of both varying effective nuclear charge and differing orbital occupation.

Plotted in Figure 4 are the $P(r_{ij})$ and $D(r_i)$ functions calculated from the configuration-interaction wavefunction of Boys. Shown in Figure 5 is $\Delta P(r_{ij})$, where

$$\Delta P(r_{ij}) = P(r_{ij})_{CI} - P(r_{ij})_{HF},$$

the shift in $P(r_{ij})$ due to the inclusion of electron correlation.

Integrals involved in the determination of the one- and two-electron distributions from all except the Boys wavefunction (52) were evaluated numerically on an IBM 7074 computer using Gauss's quadrature formula. A nonuniform grid was chosen with spacings such that further subdivision had no effect on the D(r) or P(r) curve to seven figures. The accuracy

Fig. 2. Pair distribution functions $P(r_{12})$ calculated from the correlated wavefunctions of Roothaan and Weiss for helium-like systems with nuclear charges of 2, 3, 4, 6, and 8. The functions $P(r_{12})/Z^*$ are plotted against the abscissa $Z^* r_{12}$, where Z^* is an effective nuclear charge.

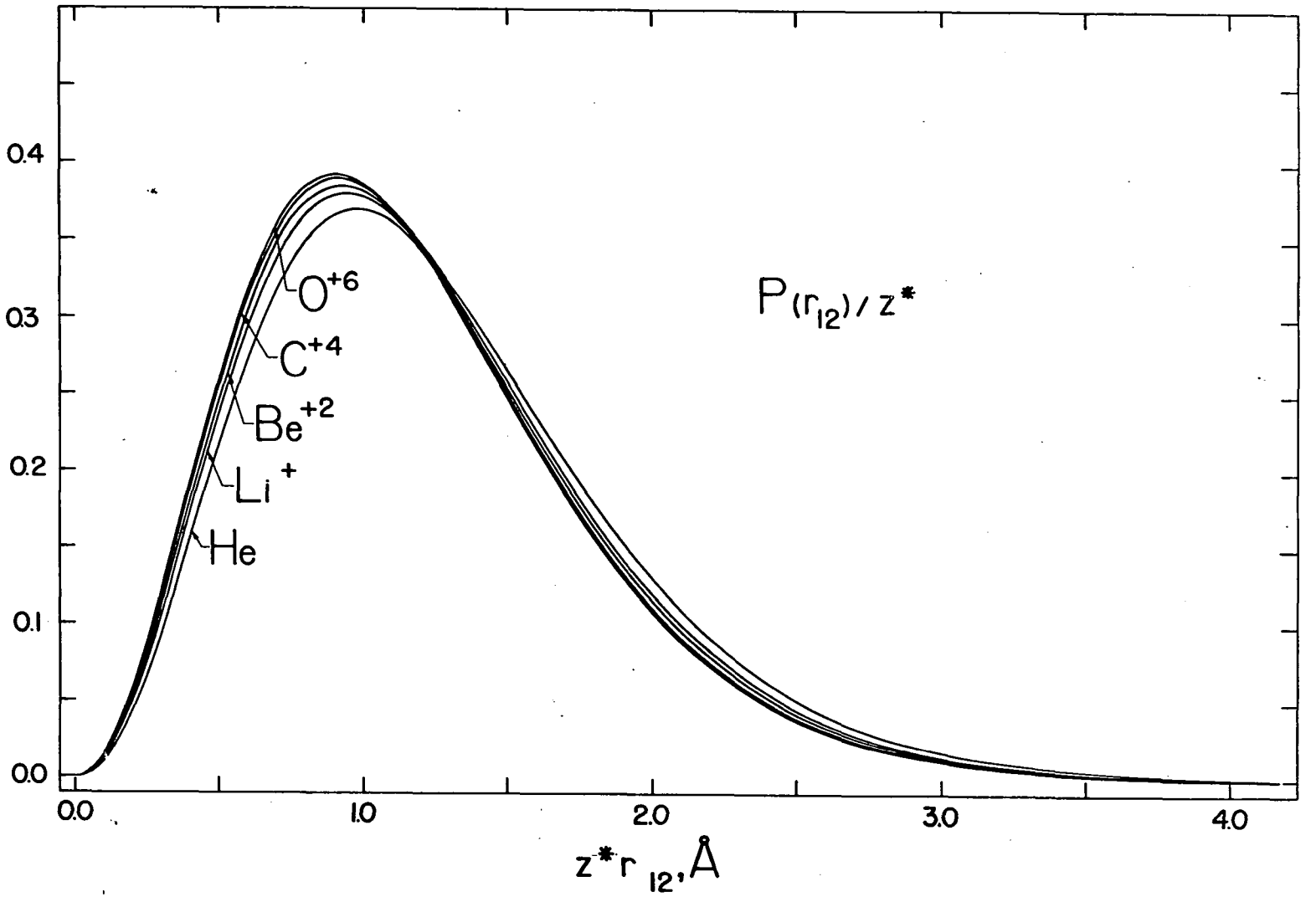
0.4
0.3
0.2
0.1
0.0
0.0
1.0
2.0
3.0
4.0
O^{+6}
C^{+4}
Be^{+2}
Li^{+}
He
$P(r_{12})/z^*$
$z^* r_{12}$, Å

Fig. 3. Differences $\Delta P(r_{12})$ between pair distribution functions calculated from correlated and uncorrelated wavefunctions plotted against the reduced radius $Z^{*}r_{12}$

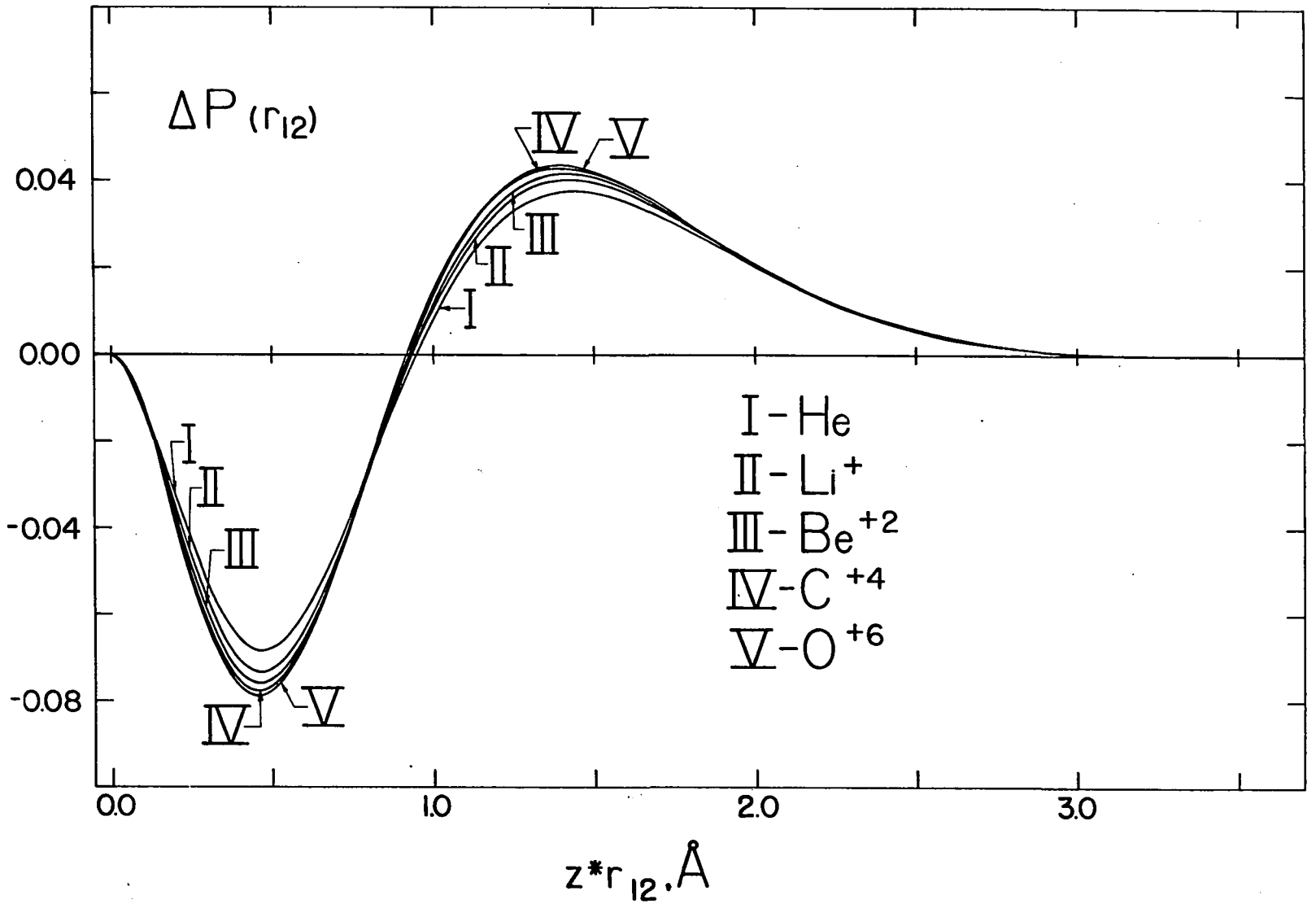
ΔP (r12)
0.04
0.00
-0.04
-0.08
0.0
1.0
2.0
3.0
z*r12, Å
I - He
II - Li+
III - Be+2
IV - C+4
V - O+6

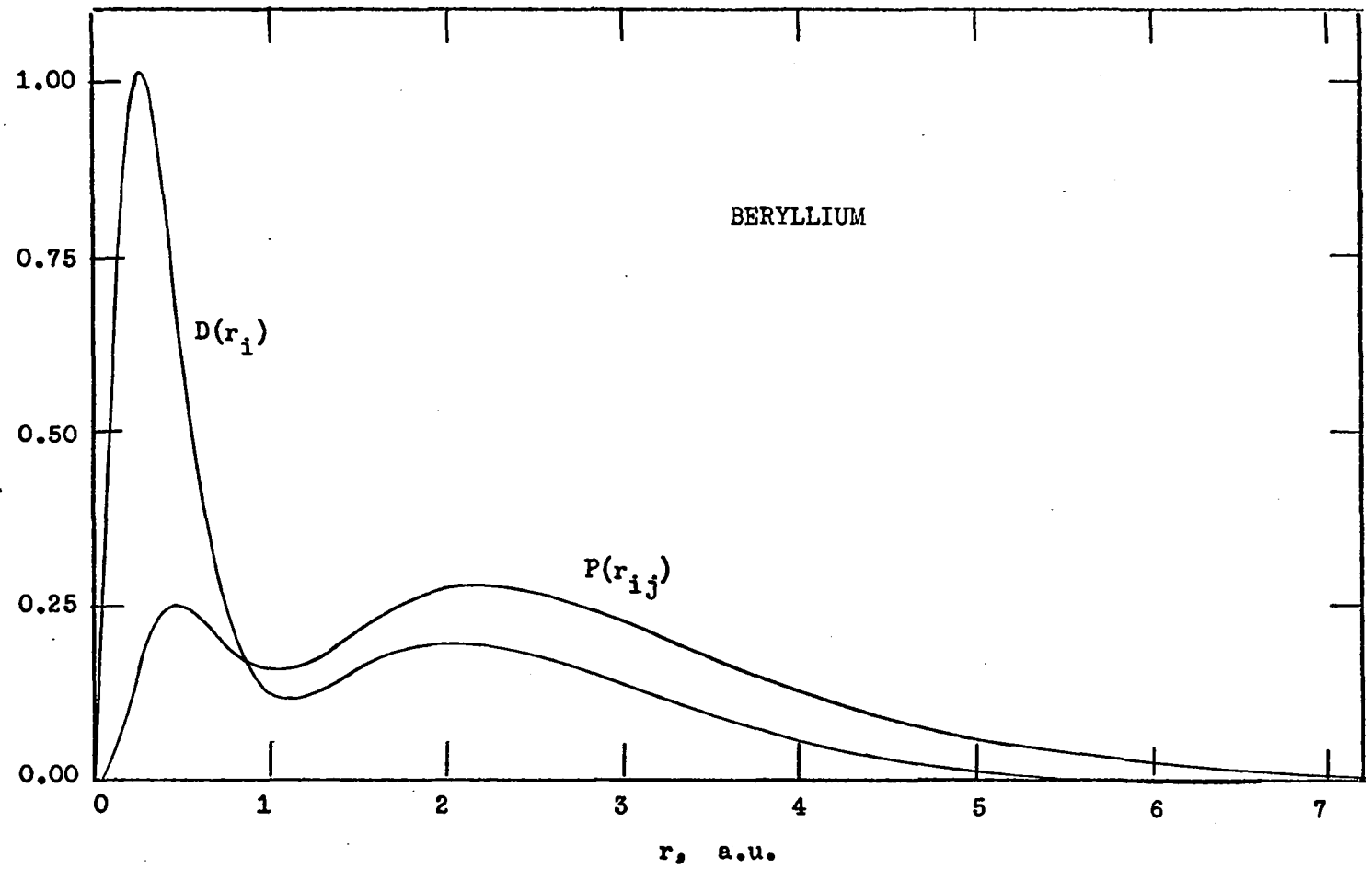

Fig. 4. Electron-nuclear $D(r_i)$ and electron-electron $P(r_{ij})$ radial distribution functions for beryllium calculated from a wavefunction due to Boys

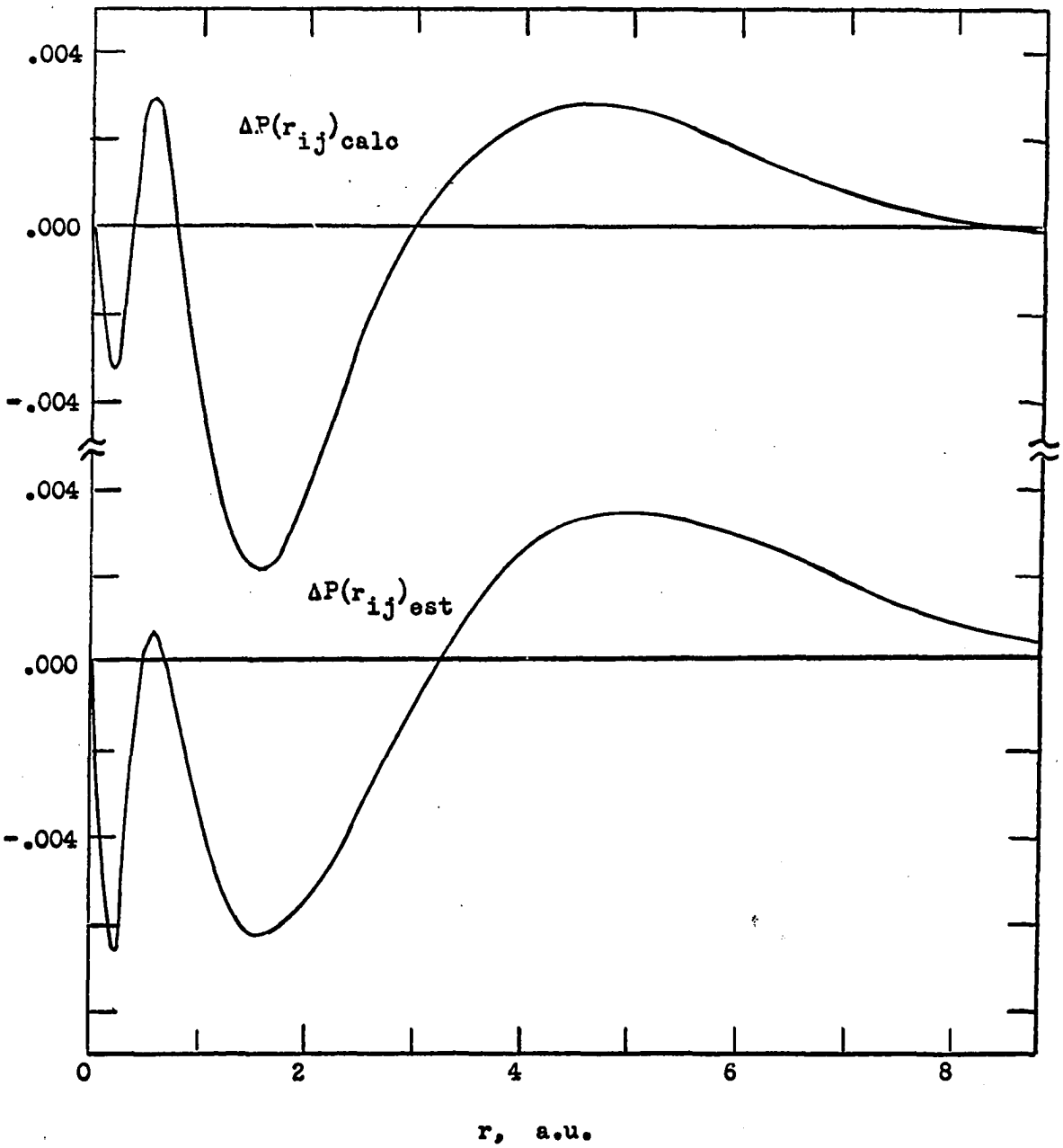

Fig. 5. Shifts in $P(r_{ij})$ due to electron correlation in the beryllium atom. The function $\Delta P(r_{ij})_{calc}$ is the difference between distribution functions calculated from correlated and uncorrelated wavefunctions. The function $\Delta P(r_{ij})_{est}$ was estimated employing the simple scheme outlined in the text.

of the results was checked by use of Equations 21, 22, and 23. In every case except O^{6+}, the energy agreed with the reported value to about five figures. For O^{6+} the energy agreed after correcting the wavefunction for a misprint in the reported expansion constants[1].

For the configuration-interaction wavefunction of Boys, analytical expressions for D(r) and P(r) were obtained by a technique suggested by Coulson and Nielson (42). The accuracy of the resulting analytical expressions was checked by calculation of all terms in the energy matrix. In each case, the calculated energy agreed exactly with the published value.

X-ray scattered intensities

The total scattered intensity of x rays is directly related to the two-electron distribution P(r) as shown by Equation 15. For helium-like systems, the intensity relationship is

$$I_{tot} = 2I_{cl}[\, 1 + \int P(r_{12})(\sin sr_{12})/sr_{12}\ dr_{12}\,], \qquad (27)$$

and the expression for the inelastic scattering factor becomes

$$S(s) = 2 + 2\int P(r_{12})(\sin sr_{12})/sr_{12}\ dr_{12} - [\int D(r)(\sin sr)/sr\ dr]^2. \qquad (28)$$

Plots of I_{tot}/I_{cl}, $F^2(s)$, and S(s) for helium are shown in Figure 6, as calculated for the Hartree-Fock and for the more exact wavefunction of

---

[1]Weiss, A. W., National Bureau of Standards, Washington, D. C., Correlated orbitals for helium-like systems. Private communication. 1964.

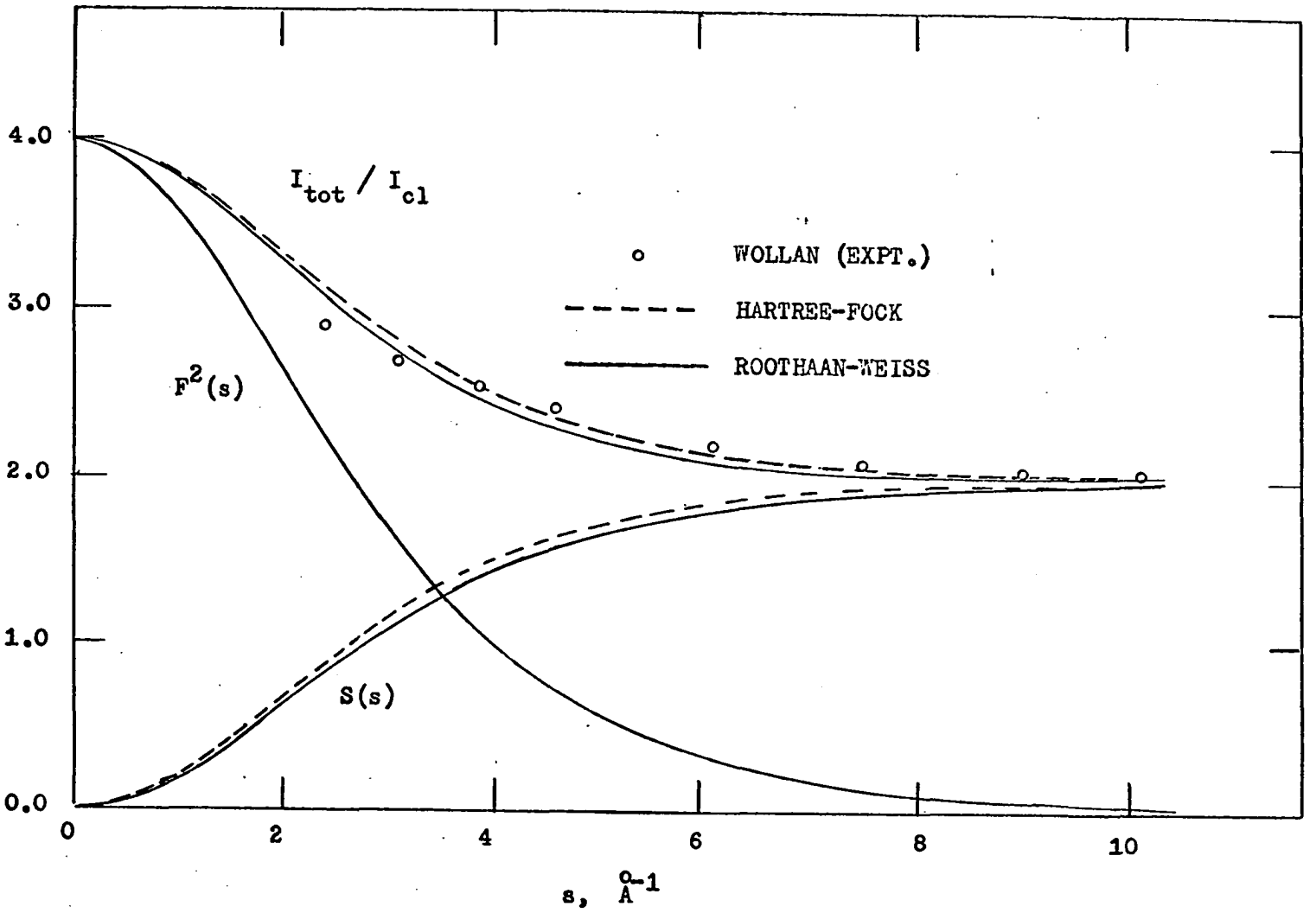

Fig. 6. Reduced total, elastic $F^2(s)$, and inelastic S(s) intensities calculated for x-ray scattered by helium. Experimental points due to Wollan are plotted as o's.

Roothaan and Weiss. It can be seen that correlation effects on the inelastic and total intensities are significant. Only one $F^2(s)$ curve was plotted in Figure 6 since the functions calculated from the two wavefunctions were indistinguishable from each other on the scale of the plot. Also plotted are the 1931 experimental values of Wollan (5), corrected for recoil effects in the inelastic scattering (37). These results are not sufficiently accurate to establish P(r) with any precision but they are not inconsistent with the present calculations.

Only recently have inelastic scattering factors derived from Hartree-Fock wavefunctions become generally available (35, 53, 54). For the most part Heisenberg-Bewilogua (33, 34) scattering factors deduced from the Thomas-Fermi statistical model have been used in the past. The statistical model may be expected to fail more seriously as the number of electrons decreases, and accurate results cannot be expected for helium. For purposes of comparison, numerical values of S(s) calculated for helium are listed in Table 1. Computations were based on Hartree-Fock (46), Hylleraas (55), and Roothaan-Weiss (47) wavefunctions.

Total, elastic, and inelastic scattered intensities for helium-like systems with atomic numbers of 3, 4, 6, and 8 were calculated from both correlated (47) and Hartree-Fock (46) wavefunctions. Numerical values of the elastic and inelastic scattering factors are listed in Table 2. The trend of correlated inelastic scattering factors S(s) as atomic number increases is shown in Figure 7, and the influence of correlation on scattered intensities is illustrated in the plot of $\Delta I/I_{cl}$ in Figure 8, where

Table 1. Inelastic scattering factors, S(s), calculated for helium

$(\sin \phi/2)/\lambda$	Statistical[a]	Hartree-Fock[b]	Hylleraas[c]	Roothaan-Weiss[d]
0.025	0.49	0.02164	0.01812	0.02052
0.050	0.79	0.08474	0.07123	0.08032
0.075	0.99	0.1841	0.1557	0.1744
0.100	1.15	0.3121	0.2659	0.2952
0.125	1.27	0.4596	0.3953	0.4348
0.150	1.38	0.6176	0.5367	0.5833
0.175	1.46	0.7779	0.6835	0.7344
0.200	1.52	0.9336	0.8297	0.8816
0.250	1.63	1.2138	1.1029	1.1385
0.300	1.70	1.4382	1.3336	1.3669
0.400	1.80	1.7275	1.6526	1.6621
0.500	1.86	1.8704	1.8241	1.8219
0.600	1.90	1.9376	1.9104	1.9052
0.700	1.92	1.9692	1.9533	1.9485
0.800	. .	1.9842	1.9747	1.9712

[a] Reference 34.

[b] 0% correlation energy, reference 46.

[c] 70.0% correlation energy, reference 55.

[d] 92.1% correlation energy, reference 47.

$$\Delta I/I_{cl} = [\,(I_{tot})_{corr} - (I_{tot})_{HF}\,]/I_{cl}$$

and $(I_{tot})_{corr}$ and $(I_{tot})_{HF}$ represent total intensities calculated from correlated and Hartree-Fock wavefunctions, respectively.

Plots of I_{tot}/I_{cl}, $F^2(s)$, and S(s) for beryllium, as calculated from the configuration-interaction wavefunction (52), are shown in Figure 9.

Table 2. Elastic and inelastic x-ray scattering factors, F(s) and S(s), calculated from correlated and Hartree-Fock wavefunctions

$(\sin \phi/2)/\lambda$	F_{corr}	F_{HF}	S_{corr}	S_{HF}	F_{corr}	F_{HF}	S_{corr}	S_{HF}
			Li^{+}				Be^{2+}	
0.05	1.9837	1.9837	0.03127	0.03246	1.9915	1.9915	0.01651	0.01700
0.10	1.9360	1.9360	0.1212	0.1258	1.9663	1.9663	0.06498	0.06691
0.15	1.8606	1.8606	0.2591	0.2691	1.9254	1.9253	0.1423	0.1466
0.20	1.7625	1.7625	0.4300	0.4468	1.8703	1.8703	0.2438	0.2511
0.25	1.6480	1.6480	0.6179	0.6421	1.8030	1.8030	0.3639	0.3748
0.3	1.5233	1.5233	0.8083	0.8398	1.7258	1.7257	0.4962	0.5110
0.4	1.2657	1.2657	1.1565	1.1991	1.5510	1.5509	0.7747	0.7974
0.5	1.0238	1.0236	1.4291	1.4761	1.3639	1.3639	1.0406	1.0699
0.6	0.8147	0.8146	1.6231	1.6682	1.1792	1.1792	1.2712	1.3047
0.7	0.6432	0.6430	1.7538	1.7932	1.0068	1.0069	1.4580	1.4931
0.8	0.5066	0.5066	1.8395	1.8717	0.8523	0.8523	1.6026	1.6367
0.9	0.3996	0.3996	1.8948	1.9202	0.7176	0.7176	1.7108	1.7425
1.0	0.3166	0.3166	1.9304	1.9499	0.6025	0.6025	1.7903	1.8185
			C^{4+}				O^{6+}	
0.1	1.9860	1.9860	0.02741	0.02797	1.9924	1.9924	0.01502	0.01524
0.2	1.9448	1.9448	0.1068	0.1089	1.9697	1.9697	0.05919	0.06008
0.3	1.8791	1.8790	0.2300	0.2347	1.9329	1.9329	0.1301	0.1320
0.4	1.7926	1.7925	0.3857	0.3935	1.8831	1.8830	0.2238	0.2271
0.5	1.6901	1.6900	0.5607	0.5720	1.8218	1.8217	0.3356	0.3406
0.6	1.5767	1.5765	0.7426	0.7573	1.7510	1.7509	0.4603	0.4672
0.8	1.3355	1.3353	1.0881	1.1085	1.5886	1.5885	0.7276	0.7284
1.0	1.1003	1.1000	1.3716	1.3950	1.4115	1.4113	0.9899	1.0041
1.2	0.8897	0.8895	1.5811	1.6044	1.2331	1.2329	1.2235	1.2400
1.4	0.7115	0.7113	1.7259	1.7470	1.0632	1.0630	1.4174	1.4350
1.8	0.4498	0.4497	1.8842	1.8989	0.7703	0.7702	1.6869	1.7034
2.0	0.3582	0.3581	1.9243	1.9359	0.6509	0.6508	1.7732	1.7882

Fig. 7. Reduced inelastic intensities S(s) for x-ray scattering by helium-like systems plotted against the reduced variable s/Z^*. Correlated wavefunctions of Roothaan and Weiss were used in the calculation of the intensities.

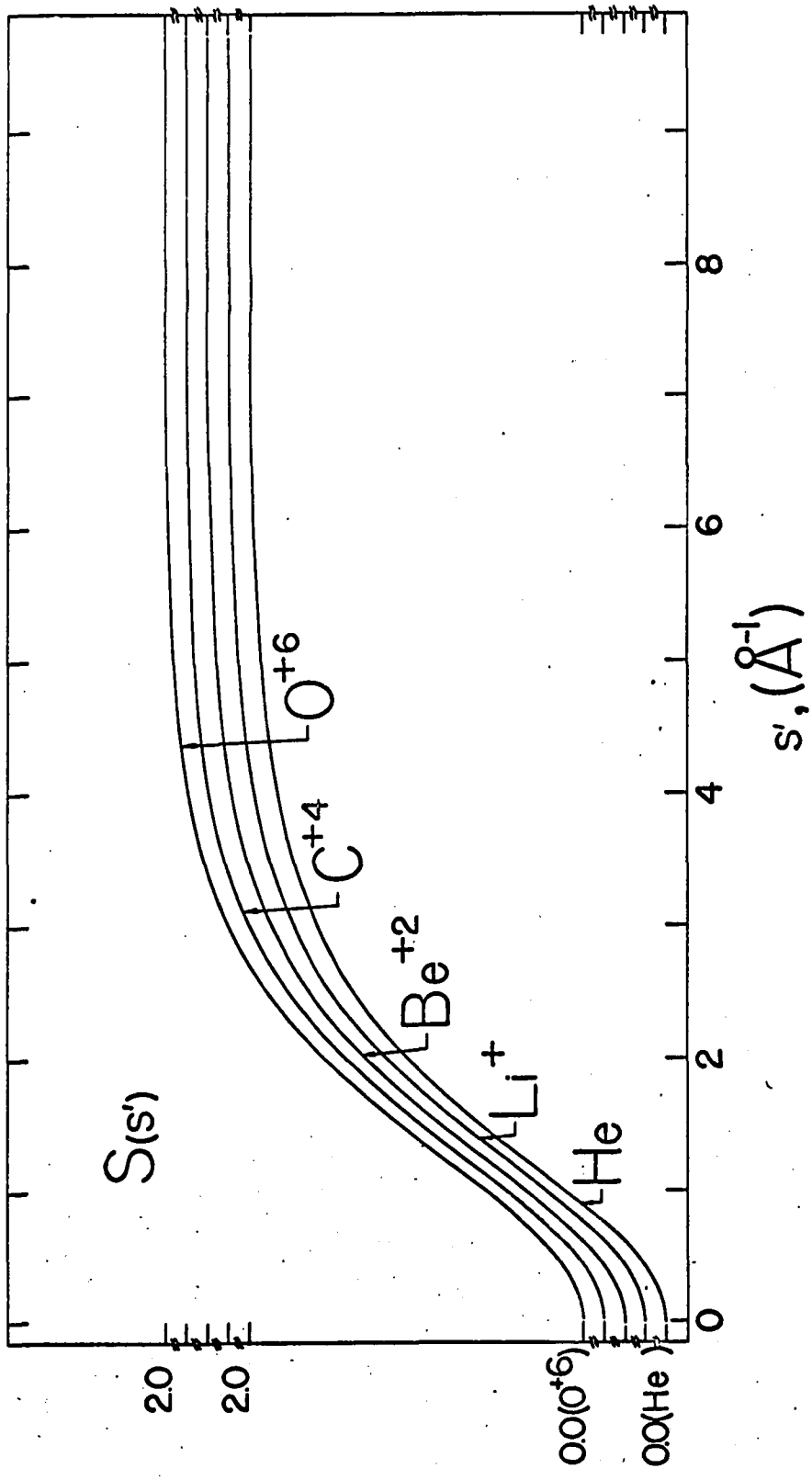
S(s')
2.0
2.0
0.0(O+6)
0.0(He)
0
2
4
6
8
s', (Å⁻¹)
O+6
C+4
Be+2
Li+
He

Fig. 8. Influence of electron correlation on total intensities of x rays scattered by helium-like systems. The functions $-Z^{*}\Delta I(s)/I_{cl}$ are plotted against the reduced variable s/Z^{*} to illustrate the scaling of the functions implicit in Equation 27.

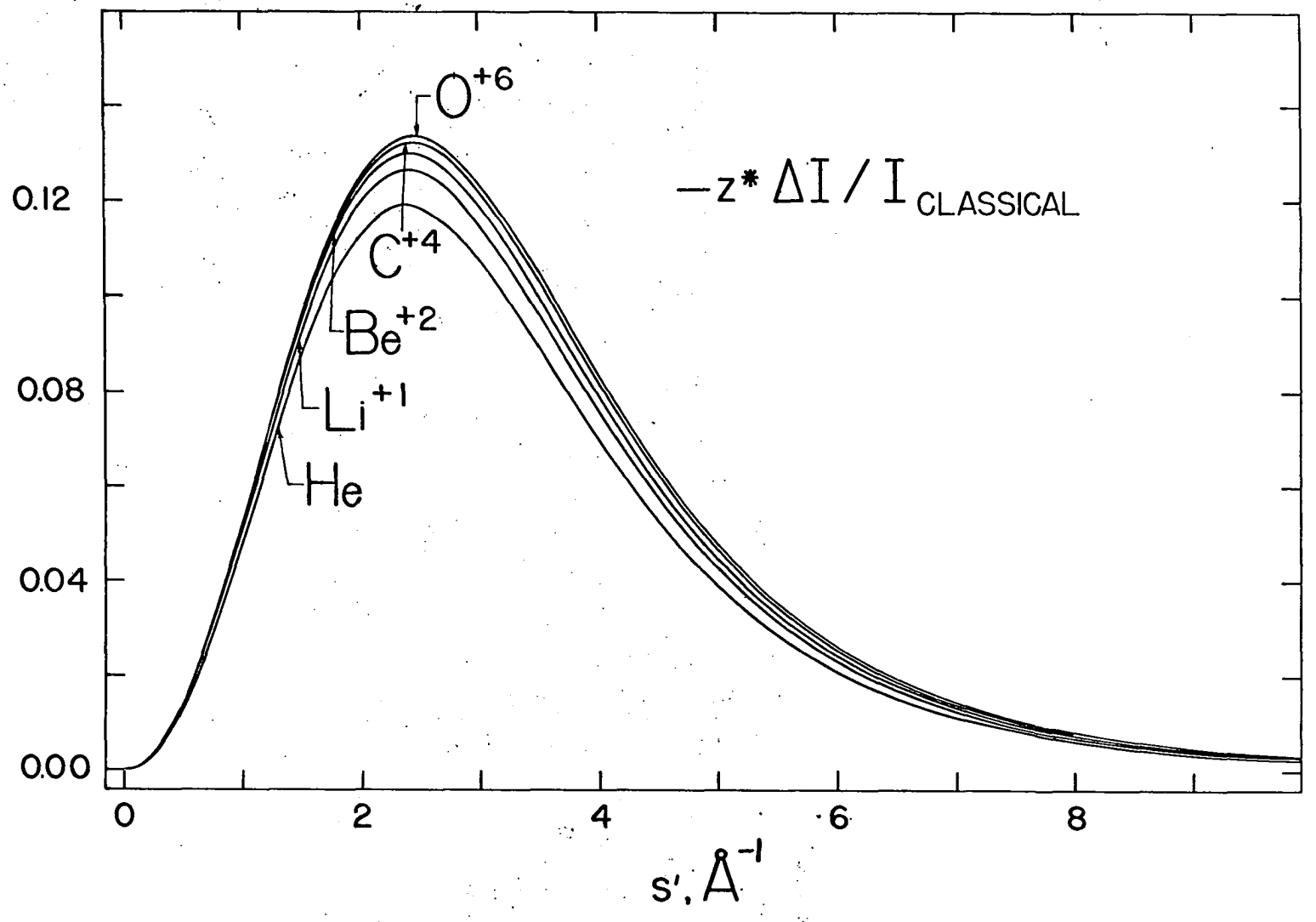
O^{+6}
C^{+4}
Be^{+2}
Li^{+1}
He
$-z^* \Delta I / I_{CLASSICAL}$
0.12
0.08
0.04
0.00
0
2
4
6
8
s', $Å^{-1}$

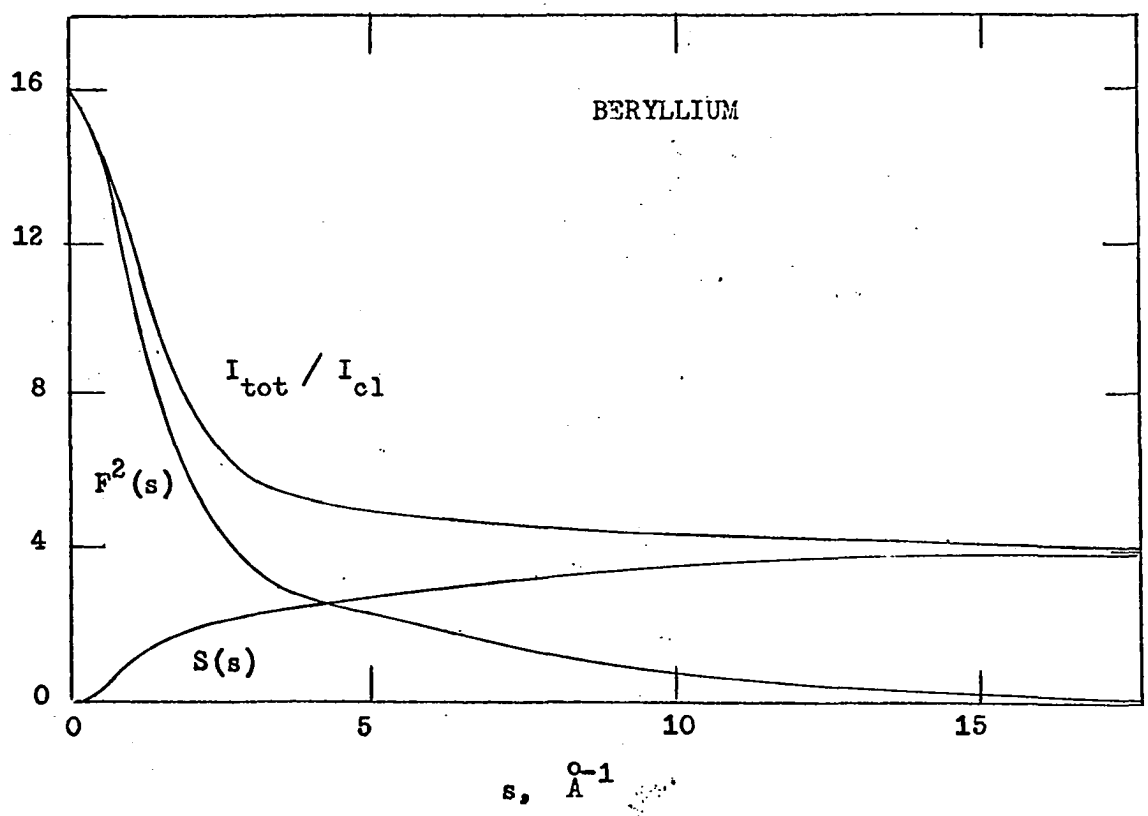

Fig. 9. Reduced total, elastic $F^2(s)$, and inelastic S(s) intensities for x-ray scattering by beryllium as calculated from a wavefunction of Boys

Plotted in Figure 10 is $\Delta I_{calc}/I_{cl}$, where

$$\Delta I_{calc} = I_{HF} - I_{CI},$$

the shift in total intensity due to correlated motions of electrons in the beryllium atom.

Discussion

The plots in Figures 1 and 3 clearly indicate that two-electron density functions are sensitive to the inclusion of correlation in the wavefunction. Shifts in the two-electron density also cause clearly discernable shifts in the total and inelastic intensities of x rays.

The electron-electron distribution curves $P(r_{12})$ for the helium-like systems calculated from the correlated wavefunctions shrink inward as the atomic number increases in the same manner as do the electron-nuclear distributions $D(r)$. As shown in Figure 2, the various $P(r_{12})$ are roughly congruent when divided by an effective nuclear charge Z^* and plotted against the product Z^*r. The effective nuclear charge adopted in plotting Figures 2, 3, 7, and 8 was the Slater rule value (56), $(Z - 0.3)$. No attempt was made to obtain an optimum value of the screening constant. Curl and Coulson (45) in an independent study of the same systems had also noted that a slightly larger value of σ in the expression $Z^* = Z - \sigma$ would lead to better scaling.

The effect of electron correlation on $P(r_{12})$, as shown in Figure 3, also shows a strikingly simple trend with atomic number. A knowledge of how rapidly $\Delta P(r_{12})$ contracts as nuclear charge increases coupled with

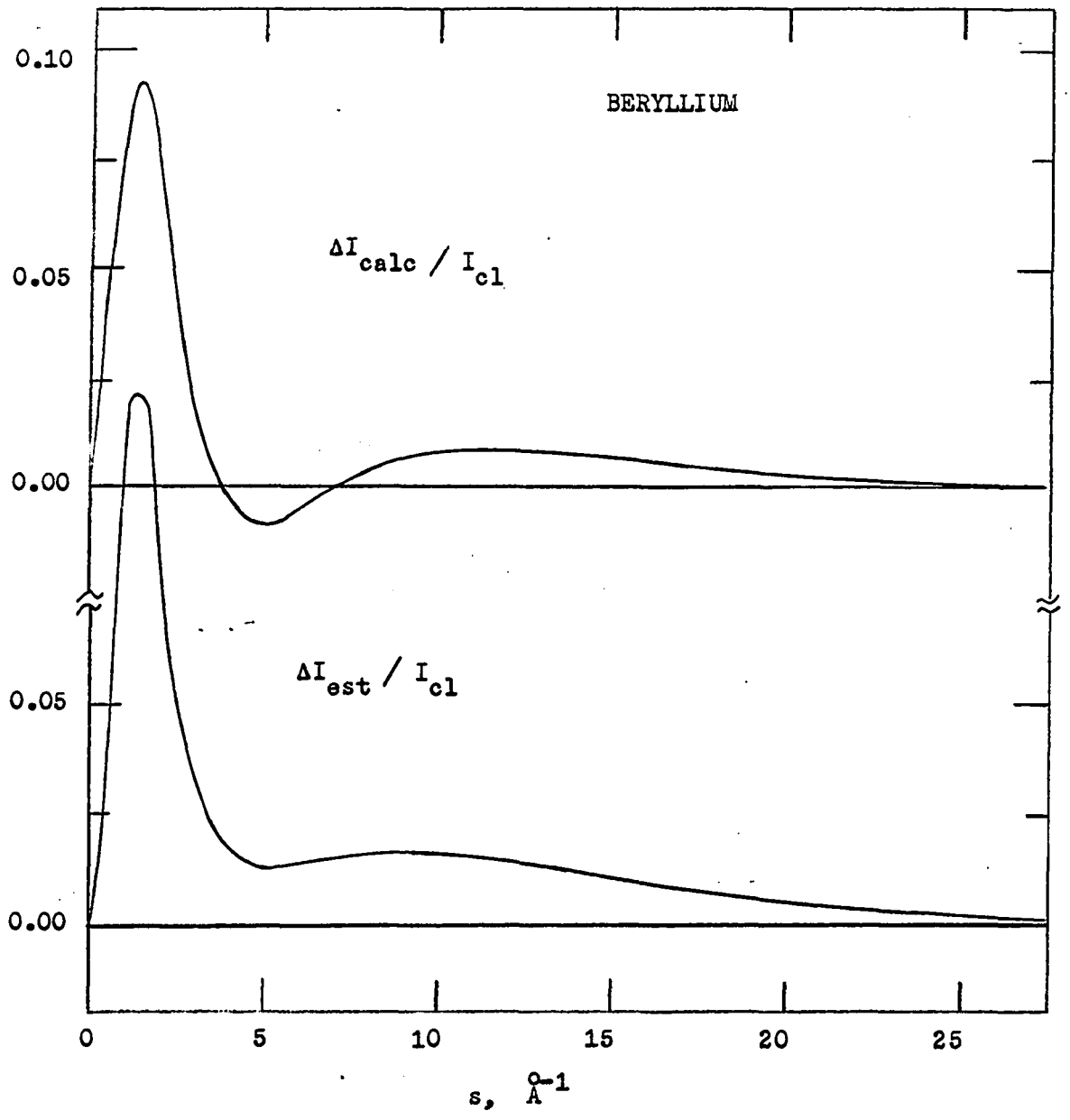

Fig. 10. The influence of correlation on the total intensity of x rays scattered from beryllium atoms. The curve $\Delta I_{calc}/I_{cl}$ was derived from intensities calculated from Hartree-Fock and correlated wavefunctions. The function $\Delta I_{est}/I_{cl}$ was estimated employing the scheme outlined in the text.

the fact that many pair correlation energies are available (57, 58, 59) should simplify the estimation of correlation effects in more complex systems.

Electron-nuclear distributions D(r) and mean potential energies $\overline{V}_{ne}$ are one-electron density functions and, accordingly, are expressed almost as well in terms of Hartree-Fock wavefunctions as in terms of properly correlated wavefunctions. It follows from Equations 21, 22, and 23 that the correlation energy is given very nearly by

$$E_{corr} \approx (1/2) \int \Delta P(r_{12})/r_{12} \; dr_{12}.$$

Since E_{corr} for the helium-like systems is almost constant (60), the integral of $\Delta P(r_{12})/r_{12}$ over all r_{12} space, or equivalently, the integral of $\Delta P(r_{12})/Z^{*}r_{12}$ over all $Z^{*}r_{12}$ space, should be constant. It is apparent from Figure 3 that not only is the integral virtually the same for all systems but the integrand itself, $\Delta P(r_{12})/Z^{*}r_{12}$, is almost invariant when expressed in terms of the reduced distance $Z^{*}r_{12}$. This is an even greater simplification for $\Delta P(r_{12})$ than might have been anticipated from the constancy of correlation energy.

From the trends illustrated in Figures 2 and 3 it appears that the zero point in the $\Delta P(r_{12})$ is closely related to the maximum of the $P(r_{12})$ function. In the event that this relationship is found to hold in general, known correlation energies will make possible simple estimations of correlation effects in $P(r_{12})$ and I_{tot} for more complex systems. If some plausible shape be adopted for a correction function $\Delta P(r_{12})$, the radial scale factor presumably can be established from the effective nuclear

charge. The remaining parameter for $\Delta P(r_{12})$, the amplitude, can be established with the aid of Equation 31.

As a first approximation, the ground state electronic wavefunction of an atom may be taken to be

$$\Psi_k = A [\lambda_1(1) \lambda_2(2) \ldots \lambda_N(N)]$$

where the $\lambda_i(i)$ are spin-orbitals from any convenient orthonormal basis set and A is the antisymmetrization operator. The expression for P(r) then may be shown to be

$$P(r) = \sum_{k}^{N} \sum_{l \neq k}^{N} P_{kl}(r)$$

where $P_{kl}(r)$ represents the pair distribution function for the k^{th} and l^{th} electrons. If we assume that the effects of electron correlation on these pair functions can be approximated by a function with a zero point at the maximum of the pair distribution curve and of the same shape shown in Figure 4, we may calculate $\Delta P_{kl}(r)$ curves by using known correlation energies to establish the amplitudes. The sum of these $\Delta P_{kl}(r)$ would then be the total effect of correlation on P(r). In addition, the effect of correlation on the total observed intensity would be

$$\Delta I = I_{cl} [\int \Delta P(r) (\sin sr)/sr \; dr].$$

A convenient, but by no means unique, choice of basis functions $\lambda_i(i)$ is the s, p, and d orbitals used by chemists. One advantage of this choice

Table 3. Pair correlation energies e_{ij} and radial values r_{max} for the maxima of the pair distribution functions in beryllium

Pair	e_{ij} (eV)	r_{max} (a.u.)	Pair	e_{ij} (eV)	r_{max} (a.u.)
1s-1s	-1.196	0.44	2s-2s	-1.195	3.25
1s-2s	-0.176	2.10			

is that numerous values for pair correlation energies have been calculated for this basis.

It is of interest then to use this scheme to predict the $\Delta P(r_{ij})$ and ΔI functions for the beryllium atom, and to compare the simple prediction with the Coulomb hole calculated from the wavefunctions. In Table 3 are found estimates of the correlation energies associated with the various electron pairs in the atom (58) and the maxima of the pair distribution functions $P_{1s,1s}$, $P_{1s,2s}$, and $P_{2s,2s}$ derived from one-electron Hartree-Fock orbitals (46). The $\Delta P(Z^{*}r_{12})$ function employed in the calculations was that of the Be^{2+} ion.

Plotted in Figure 5 are the $\Delta P(r_{ij})$ curve calculated from the wavefunctions and the $\Delta P(r_{ij})$ predicted using the simple scheme outlined above. The corresponding shifts in the total intensity, both calculated and predicted, are shown in Figure 10.

The general shape of the predicted and calculated functions are the same. The base lines, however, are not the same for both. The possibility

exists that the principal discrepancy between predicted and calculated functions is a result of the correlated wavefunction including only 50% of the correlation energy. Only more detailed calculations could verify this supposition. In any case, it appears that the simple scheme provides at least a rough estimate of the shape of the Coulomb hole from which gross estimates of effects of Coulomb correlation on scattered intensities can be deduced.

The rough agreement between simple approximation and theoretical calculations implies that the largest relative effects on x-ray scattering may be expected for shells of smallest effective nuclear charge and greatest radius in the atom. The correlation effect on inelastic scattering at small angles by K electrons diminishes from about 6% for helium to about 1% for oxygen. At large angles S(s) approaches the number of electrons causing the scattering irrespective of nuclear charge or correlation. In many electron atoms it is likely that precise measurements of intensities of inelastically scattered x rays will reveal effects of several percent, in comparison to Hartree-Fock calculations, attributable to correlation effects on valence electrons. Inner-shell effects will be smaller and delocalized over a greater range of s, and will be correspondingly very much more difficult to detect.

For a two electron system, a meaningful study of electron correlation itself could be made rather than simply a study of observables influenced by correlation. From elastic intensities it is possible, in principle, to determine the electron-nuclear radial distribution function $D(r_i)$. From $D(r_i)$, in turn, it is possible to construct a product wavefunction which reproduces this $D(r_i)$. Such a wavefunction should correspond

closely to a Hartree-Fock function because Hartree-Fock $D(r_i)$ distributions are almost indistinguishable from exact distributions (48, 49, 50, 51). Accordingly, a $P(r_{12})$ function could be calculated from the "experimental Hartree-Fock" function and compared with the experimental $P(r_{12})$ function derived from the total intensity. In this way an experimental determination of the Coulomb hole is possible.

Expressions for electron diffraction studies of gas atoms and molecules which are analogous in form to Equations 13 and 17 may be derived by making assumptions somewhat more severe than those for x-ray diffraction. As in the case of x rays, the model considered is nonrelativistic with the incident energy large compared with excitation energies. If polarization and exchange are ignored, expressions for intensity paralleling Equations 1 and 2 for x rays result (61). The only adjustments which must be made are that nuclei as well as planetary electrons scatter wavelets, but with amplitudes -Z times as great, and that I_{cl} for electrons is given by the Rutherford scattering law (62) rather than the Thomson equation (36).

For a gas molecule, the intensity expression for an average over random orientation of the molecules is exactly analogous to Equation 17 (63), or

$$I_{tot} = I_{cl}^{R} \sum_{\mu} \sum_{\nu} Z_{\mu} Z_{\nu} \int P_{\mu\nu}(r) \, (\sin sr)/sr \; dr \qquad (29)$$

where the sum is over all particles, nuclei and electrons alike, with Z_{μ} standing for atomic number if μ is a nucleus and standing for -1 if μ is an electron, and I_{cl}^{R} is the Rutherford intensity (62). For a gas atom,

Equation 29 reduces to

$$I_{tot} = I_{cl}^{R} \left[Z^2 - 2Z \sum_i \int D(r_i)(\sin sr_i)/sr_i \, dr_i \right.$$

$$\left. + \sum_i \sum_j \int P(r_{ij})(\sin sr_{ij})/sr_{ij} \, dr_{ij} \right] \qquad (30)$$

in which i and j denote electrons. Equation 30 may be reduced to the conventional electron diffraction expression for atoms by use of Equations 4, 13, and 15, or

$$I_{tot} = I_{cl}^{R} \left[(Z-F(s))^2 + S(s) \right]. \qquad (31)$$

The corresponding expression for the elastic intensity is

$$I_{elas} = I_{cl}^{R} \left[Z - F(s) \right]^2.$$

Effects of electron correlation are manifested, therefore, in the total intensity of electrons scattered from gas atoms. The greater uncertainty of the theory, as discussed above, detracts from the feasibility of these studies employing electron diffraction. It is interesting to note, however, that the expression for inelastic scattering of electrons is probably not sensitive to errors in the Born approximation (63). The Born approximation gives the correct expression for the intensity scattered by an isolated charged particle even though it gives incorrect phases of the scattered waves. It also gives essentially correct interference terms for the scattering by a system of particles of identical

charge. It gives incorrect interference terms for a pair of particles of significantly different charge. The electron-electron terms of Equation 30, which include inelastic scattering, are probably accurate. The electron-nuclear terms are less reliable but, since they contribute only to the elastic scattering, their uncertainty is less serious in correlation studies.

Further applications of this general approach in electron diffraction have been discussed by Bonham, et al. (61, 64).

Experimental Distribution Functions

Method

Earlier in this dissertation it was pointed out that experimental studies of x-ray scattering by gas atoms can reveal not only D(r), the radial distribution of electrons around nuclei, but also P(r), the radial distribution of electrons with respect to other electrons. In experimental work published to date (4, 6, 7, 8) attention has been focused only on the simplier property D(r), a property which can be calculated quite easily with considerable accuracy because it is insensitive to electron correlation. The distribution P(r) is intrinsically much more interesting, however, because its form depends on electron correlation, the major stumbling block to accurate quantum calculations.

Intensity expressions for scattering of high energy x rays, according to the nonrelativistic approach of Waller and Hartree (2), were given in Equations 13 and 17. These expressions were derived neglecting recoil effects in the inelastic events and assuming an infinite incident beam energy, however, and corrections to experimental data may be necessary to

compensate for these deficiencies. An alternative expression for the total intensity, including correction for recoil, is (37, 65)

$$I_{tot} = I_{cl} [F^2(s) + Q S(s)] \quad (32)$$

where Q, a correction for recoil in the inelastic events as discussed by Breit (66) and Dirac (67), is equal to $[1 + \lambda h s^2/8\pi^2 mc]^{-3}$ and h is Planck's constant, m the mass of an electron, and c the velocity of light. If Q is taken to be unity, Equation 32 becomes identical to Equation 13. Because of assumptions mentioned earlier, if x-ray energies are not sufficiently high in comparison with energies of allowed electronic transitions, Equations 32 and 17 are only approximately correct. Bonham has shown how corrections for this source of error may be made (68). If suitable corrections are made to I_{tot} for effects of recoil and finite incident beam energy, experimental P(r) functions may be deduced from intensity measurements by taking a Fourier sine transform as shown in Equations 17 and 19.

The lack of experimental data for s values larger than $4\pi/\lambda$ necessitates the use of an extrapolation procedure to obtain the Fourier sine transform of the observed intensities. The method chosen in the present investigation of P(r) was similar to one proposed by Hauptman and Karle (39) in studies of D(r) and involved the fitting of experimental intensity data with an analytical function of the form

$$I_{cal}/I_{cl} = N + \sum_{i=1} a_i/(1+b_i s^2)^1 i. \quad (34)$$

The constants b_i and l_i are positive numbers and N is the number of electrons in the atom. Hauptman and Karle restricted the a_i values to positive numbers in order to insure a non-negative distribution function. In the present calculations, however, the only restriction placed on the a_i was that the distribution generated by the analytical function be non-negative. The relaxation of the restriction that a_i be positive allowed more rapid convergence of the parameters and a better fit of the data. The constants a_i and b_i for the best fit were obtained by use of the Gauss-Newton method of least squares. Calculations were repeated several times with different choices of l_i and n in order to obtain accurate fits with a reasonable number of terms and to determine the sensitivity of the fitting procedure to the set of functions adopted. An indication that the functions were adequately flexible was provided in fits of theoretical intensities. Deviations in these fits were negligible in comparison with the scatter of experimental data points.

Once the parameters of Equation 34 are determined, the Fourier inversion required to obtain P(r) can be done analytically. The resulting functions are given explicitly by Hauptman and Karle (39).

The experimental data chosen were those of Laurila (69). More accurate data are available over a limited range of scattering variable (70) but the Laurila data are the most accurate data which span a sufficient range of s to allow the Fourier inversion to be carried out definitively over the desired range of r. Corrections for recoil effects in the inelastic intensity were made by means of the relation

$$I_{tot}/I_{cl} = [I_{exp}/I_{cl}] + (Q - 1)[(I_{exp}/I_{cl}) - F(s)^2]. \quad (35)$$

Values of F(s) for neon and argon were taken from the work of Freeman (71) and Berghius, et al. (72), respectively. The corrections were small and insensitive to the exact form of F(s). No corrections were made for the effect of the limited beam energy (68).

Results

Experimental x-ray intensities for neon and argon reported by Laurila (69) are given in Table 4 along with intensity values corrected according to Equation 35. Analogous theoretical values constructed from self consistent field inelastic (73) and elastic (71) scattering factors are listed in Table 5. The theoretical and corrected experimental values were fitted by analytical functions of the form specified in Equation 34. In the case of the experimental data, an extra unobserved point $I_{tot}(0)/I_{cl} = Z^2$ was added to aid in the attainment of a reasonable behavior as s approached zero. Although an intercept of Z^2 is demanded by theory, an uncertainty exists in the experimental vertical scale factor. Therefore, the assumed data point at s = 0 was no more heavily weighted in least-squares fittings than the other data points. The resulting parameters of the curve fittings are shown in Table 6. Numerical values calculated from the analytical representations are listed in Table 4.

The associated electron-electron radial distribution functions $P(r_{ij})$ derived from the experimental data and from the correlationless theoretical intensity values are plotted in Figures 11 (b) and 12 where

Table 4. Experimental x-ray intensities for neon and argon derived from Laurila's data. The reduced quantities I_{exp}/I_{cl}, I_{tot}/I_{cl}, and I_{cal}/I_{cl} represent, respectively, original experimental values, values after correction for recoil, and values calculated from a flexible analytical function adjusted by least squares to fit I_{tot}/I_{cl}

$(\sin \phi/2)/\lambda$	I_{exp}/I_{cl}	I_{tot}/I_{cl}	I_{cal}/I_{cl}	I_{exp}/I_{cl}	I_{tot}/I_{cl}	I_{cal}/I_{cl}
		Neon			Argon	
0.0000	100.0	100.0	100.15	324.0	324.0	323.91
0.1229	83.20	83.20	82.45	250.0	250.0	250.92
0.1536	74.40	74.40	74.53	222.3	222.3	221.08
0.1841	65.25	65.25	66.40	192.6	192.6	192.47
0.2146	58.40	58.40	58.46	166.1	166.1	166.68
0.2449	52.35	52.35	51.08	144.4	144.4	144.75
0.2751	44.50	44.50	44.45	127.4	127.4	126.78
0.3053	38.25	38.25	38.65	112.0	112.0	112.46
0.3352	33.10	33.10	33.77	101.0	101.0	101.40
0.3650	29.90	29.90	29.71	93.96	93.96	92.90
0.4241	24.40	24.40	23.73	81.36	81.37	81.29
0.4824	19.72	19.73	19.86	73.80	73.81	73.89
0.5398	17.00	17.01	17.30	67.50	67.51	68.37
0.5960	15.33	15.34	15.53	63.72	63.74	63.62
0.7052	13.39	13.41	13.19	55.71	55.73	54.93
0.8089	12.01	12.04	11.75	46.89	46.92	47.32
0.9065	10.78	10.82	10.86	41.49	41.53	41.12
0.9972	10.06	10.10	10.34	35.82	35.88	36.35

Table 5. Reduced intensity values I_{tot}/I_{cl} for neon and argon calculated from elastic and inelastic scattering factors

$(\sin \phi/2)/\lambda$	Neon	Argon
0.0	100.0	324.0
0.1	88.48	271.4
0.2	63.75	179.4
0.3	41.31	116.6
0.4	26.94	84.67
0.5	19.13	68.46
0.6	15.12	58.72
0.7	13.06	51.43
0.9	11.41	39.19
1.1	10.90	30.12

Table 6. Constants derived from least-squares fits of experimental and theoretical intensity values using the function specified by Equation 34

l_i	a_i	b_i	l_i	a_i	b_i
	Neon				
	Experimental			Theoretical	
2	10.26	0.01107	2	27.31	0.02235
6	60.16	0.02897	6	-62.17	0.02343
6	47.54	0.00449	6	-45.92	0.006936
6	-316.26	0.01190	6	462.59	0.01208
6	562.65	0.01510	6	-673.62	0.01425
6	-253.68	0.02056	6	381.81	0.01809
	Argon				
	Experimental			Theoretical	
2	351.29	0.01999	2	368.33	0.02172
4	241.23	0.03623	4	305.49	0.04129
6	87.99	0.006195	6	-445.17	0.008333
6	649.97	0.00950	6	-1366.0	0.01764
6	-1024.58	0.008442	6	1443.3	0.01608

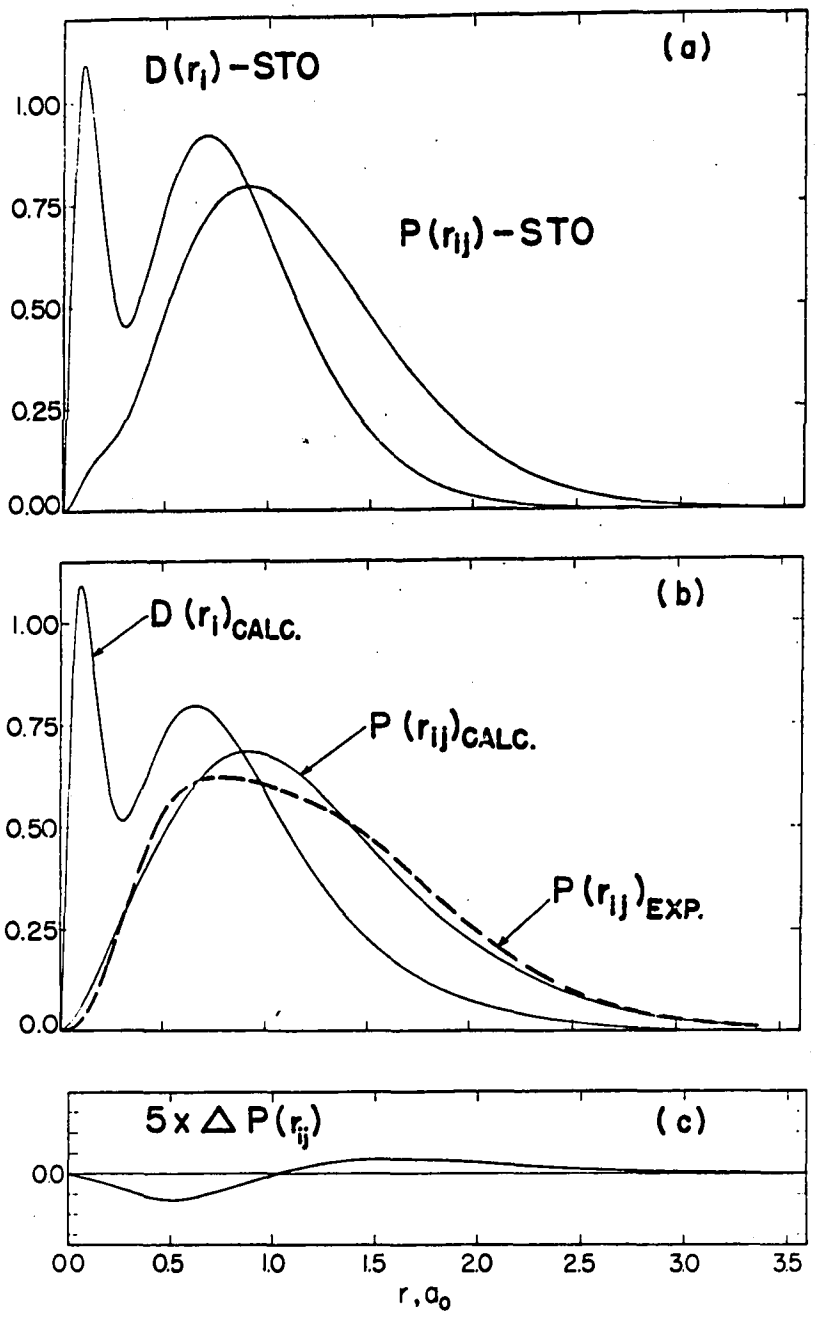

Fig. 11. Nuclear-electron $D(r_i)$ and electron-electron $P(r_{ij})$ radial distribution functions for neon. (a) Distributions calculated from single determinant wave function based on orthogonalized Slater-type orbitals with exponents optimized by Tubis. (b) Light lines represent distributions calculated from self consistent field wave functions. Heavy dashed line represents $P(r_{ij})$ derived from Laurila's experimental x-ray study. (c) Rough estimate of the effect of electron correlation on $P(r_{ij})$. $\Delta P(r_{ij})$ is enlarged five-fold in comparison with the other functions.

Fig. 12. Nuclear-electron $D(r_i)$ and electron-electron $P(r_{ij})$ radial distribution functions for argon. Light lines represent distributions calculated from self consistent field wavefunctions. Heavy dashed line represents $P(r_{ij})$ derived from Laurila's experimental x-ray study.

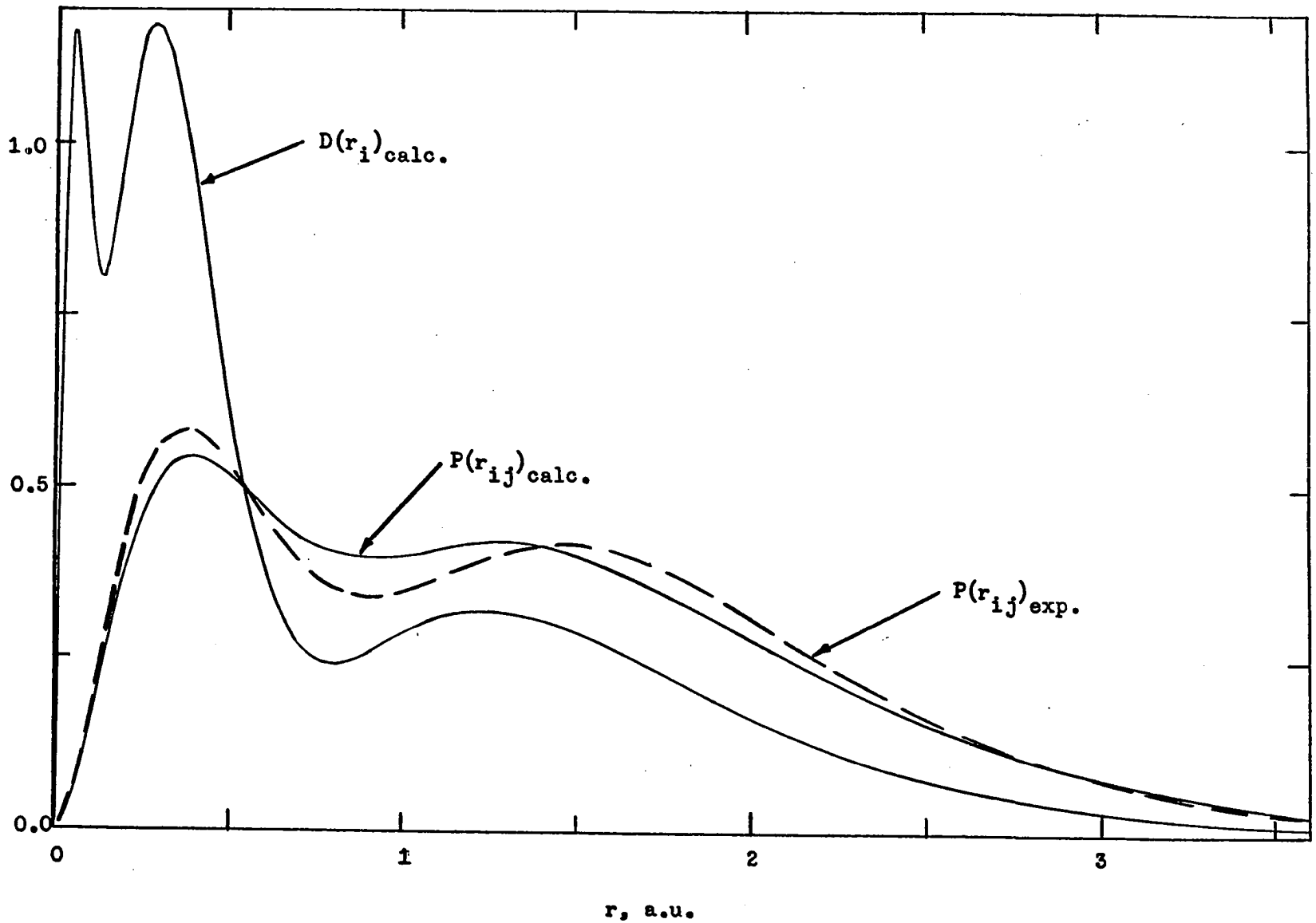
1.0
0.5
0.0
0
1
2
3
r, a.u.
$D(r_i)_{calc.}$
$P(r_{ij})_{calc.}$
$P(r_{ij})_{exp.}$

they are compared with conventional electron-nuclear radial distribution functions, $D(r_i)$. The wavefunctions from which the neon and argon $D(r_i)$ were calculated were analytical self consistent field functions due to Allen (74) and to Watson and Freeman (75), respectively. Figure 11 (a) depicts the theoretical $P(r_{ij})$ and $D(r_i)$ calculated for neon from a single determinant wavefunction in which individual atomic orbitals were taken to be orthogonalized Slater-type orbitals with exponents optimized by Tubis (76).

It is of interest to determine whether x-ray diffraction is likely to be of practical value in deriving electron distributions in atoms. It is not immediately obvious from a comparison of the experimental and self consistent field theoretical distributions whether the discrepancies are due to experimental error or to correlation effects. In order to help resolve this question, the influence on $P(r_{ij})$ of experimental uncertainties and, in addition, the effects of electron correlation were investigated. The correlation effects were estimated using the technique described earlier in this dissertation. Values of the pair correlation energies were estimated from the energy values of Clementi (59) and the $\Delta P(Z^* r_{12})$ used as a reference curve was that of the Be^{2+} ion. The predicted effects of correlation, which are portrayed in Figure 11 (c), must be regarded as speculative but the order of magnitude is probably not in error.

Rough estimates of the uncertainty in the experimental $P(r_{ij})$ functions due to scatter of the data points and to the restricted angular range were made. For neon the uncertainties were approximately 0.05 from interelectronic distances of 0.2 to 1.0 a.u. and 0.03 from 1.0 to 2.5 a.u.

For argon they were 0.04 from 0.25 to 1.0 a.u. and 0.03 from 1.0 to 2.2 a.u. The lack of experimental data for small and for large scattering angles prevents an accurate estimation of $P(r_{ij})$ outside $r_{ij} = 2.5$ and inside $r_{ij} = 0.2$ a.u. The values shown for the experimental curves at large radii are determined by the exact form of the somewhat arbitrary analytical functions of Equation 34 in the unobserved small angle scattering region. The values for small radii are exceedingly sensitive to the choice of vertical scale factor selected in the reduction of the experimental arbitrary intensity values to values appropriate for comparison with theoretical. This scale factor determines the speed with which the corrected experimental intensity values appear to approach the asymptote Z at large scattering angles. It governs, accordingly, the speed with which $P(r_{ij})$ appears to vanish as r_{ij} approaches zero. The angular range over which scattered intensities must be measured in studies of $P(r_{ij})$ is similar to the range required for $D(r_i)$. Such requirements are discussed by Bartell and Brockway (77).

Discussion

The experimental electron-electron distribution functions are of a very reasonable shape and, indeed, in the case of neon at least, seem to be more accurate than $P(r_{ij})$ distributions calculated from simple Slater-type orbital determinant wavefunctions. The Slater-type orbital peaks shown in Figure 11 (a) are not as diffuse as the actual peaks in $D(r_i)$ and $P(r_{ij})$ functions. On the other hand, the curves in Figure 11 (b), together with the error estimates in the previous section, indicate that the Laurila data are not reliable enough to show effects of electron

correlation.

It is possible to derive mean electron-electron contributions V_{ij} to the potential energy by averaging the electron-electron repulsion term $1/r_{ij}$ over the $P(r_{ij})$ function. A sum of V_{ij} over all pairs of electrons yields the total electron-electron potential energy in an atom. The V_{ij} for neon and argon calculated from the analytical fits of the experimental data are 1.12 a.u. and 1.40 a.u., respectively. Corresponding values of 1.20 a.u. and 1.36 a.u. were calculated from the wavefunctions studied (74, 75). This comparison strengthens the conclusion that the experimental $P(r_{ij})$ functions are qualitatively quite satisfactory but quantitatively uncertain by an amount greater than the correlation effect.

In the case of helium the relative vertical shift in $P(r_{12})$ due to electron correlation is about 10% over a large range of r_{12}, giving a maximum shift of about 0.06 in $P(r_{12})$. Therefore, x-ray data for helium accurate to, say, 2% over a reasonable range of scattering variable could determine an experimental $P(r_{12})$ function of appreciably greater accuracy than a Hartree-Fock function. Polyelectron atoms present more of a problem. Correlation effects on intensity increase roughly linearly with N, whereas the intensity itself increases approximately with the square of N. Therefore, correlation effects on individual terms $P(r_{ij})$ get diluted as N increases. The average correlation effect in the $P(r_{12})$ of helium with $N = 2$ is about 0.03 from $0 < r_{12} < 2$. The characteristic uncertainty of about 0.04 in the $P(r_{ij})$ calculated from available data for neon ($N = 10$), and argon ($N = 18$) suggests that it will not be a simple matter to derive experimental distributions in polyelectron systems

that are comparable in accuracy to Hartree-Fock distributions. Recently x-ray data accurate to 1/4% over a limited range of scattering angle have been obtained by Chipman and Jennings (70). If data of this accuracy could be obtained over a considerably larger range of s, experimental documentation of Coulomb hole functions would be possible for at least the lighter atoms.

ELECTRON DIFFRACTION STUDY OF XENON HEXAFLUORIDE

Theoretical Expressions

Theoretical expressions for the scattering of high energy electrons by molecules were developed by Mott (78), Wierl (79), and Debye (80). Corrections for anharmonicity of vibration (81), failure of the Born approximation (82, 83, 84), and finite beam energy (68) have been added to the original expressions in recent years.

When high energy electrons encounter a molecule they are scattered by both planetary electrons and atomic nuclei. The total observed intensity may be separated into that scattered from the individual atoms, I_{at}, and that resulting from the geometric arrangement of the atoms in the molecule, I_{mol}. If the energy of the incident electrons is assumed to be large in comparison with energy differences between bound states of the system, the contribution from atomic scattering may be given as

$$I_{at} = (K/s^4) \left[\sum_i (Z_i - F_i(s))^2 + S_i(s) \right] \qquad (36)$$

where the sum is taken over all atoms in the molecule, $F_i(s)$ and $S_i(s)$ represent the elastic and inelastic x-ray scattering factors for atom i, respectively, and K is related to the incident beam intensity, the number of atoms encountering the beam, and the distance between the point of interaction and the point of observation (77). The contribution from molecular scattering, under the same energy conditions, may be given as

$$I_{mol} = (K/s^4) \sum_i \sum_j{}' [Z_i - F_i(s)][Z_j - F_j(s)] \int_0^\infty P_{ij}(r)(\sin sr)/sr \, dr \qquad (37)$$

where the double summation is over all i and j except for i=j and $P_{ij}(r)$ is the probability distribution function for the separation of the i^{th} and j^{th} atomic nuclei.

It is convenient in structural studies to work with a reduced intensity function M(s), where

$$M(s) = I_{mol}/I_{at} = [(I_{tot}/I_{at}) - 1].$$

If the $P_{ij}(r)$ are approximated by Morse distribution functions (86), and corrections for failure of the Born approximation included (82), the theoretical reduced intensity function may be expressed as

$$M_{th}(s) = \sum_i \sum_j{}' C_{ij}U_{ij}(s) \exp(-(l_m^2)_{ij}s^2/2) (\cos \Delta n_{ij}) \times \sin s(r_g(1)_{ij} + \phi(s)_{ij})/s(r_e)_{ij} \qquad (38)$$

where

$$C_{ij} = Z_iZ_j/\sum_k (Z_k^2 + Z_k),$$

$$U_{ij}(s) = [Z_i - F_i(s)][Z_j - F_j(s)]/[C_{ij}(\sum_k (Z_k-F_k(s))^2 + S_k(s))],$$

$(l_m)_{ij}$ is the effective root mean square amplitude of vibration of the ij^{th} atom pair (87), $(\cos \Delta n_{ij})$ is the phase shift correction for failure of the Born approximation (82), $r_g(1)_{ij}$ is the center of gravity of the ij^{th} distribution $P_{ij}(r)/r$ (87), $\phi(s)_{ij}$ is the frequency modulation term associated with the ij^{th} anharmonic oscillator (87), and $(r_e)_{ij}$ is the

equilibrium distance for the ij^{th} atom pair.

Method of Analysis

Apparatus

The electron diffraction apparatus used in this experiment was constructed at Iowa State University and has been described in the literature (88). It is similar in many ways to the electron diffraction unit at the University of Michigan (89). A schematic diagram is shown in Figure 13.

A heated filament is used for the electron source. Electrons emitted from this filament are accelerated through a potential difference of 40,000 volts and are focused by a magnetic lens in the instrument. Diffraction patterns are obtained by intersecting the focused beam of electrons with a narrow stream of gas molecules. Scattered electrons are recorded on four by five inch Kodak process plates and heart-shaped rotating sectors are used to compensate for the rapid falloff of intensity with increasing scattering angle (85).

Data were taken at two different camera lengths, 21 cm. and 11 cm., using a sector with an angular opening proportional to the cube of the sector radius. In order to obtain accurate data for small scattering angles, pictures were taken at the 21 cm. camera distance using a sector with an angular opening proportional to the square of the radius. Camera distances were measured with a cathetometer and reliable data were obtained for the range $2.5 < s < 39.1$.

A XeF_6 sample of 99.8 mole-percent purity was provided by Dr. C. L. Chernick of Argonne Labs. It was contained in a specially constructed

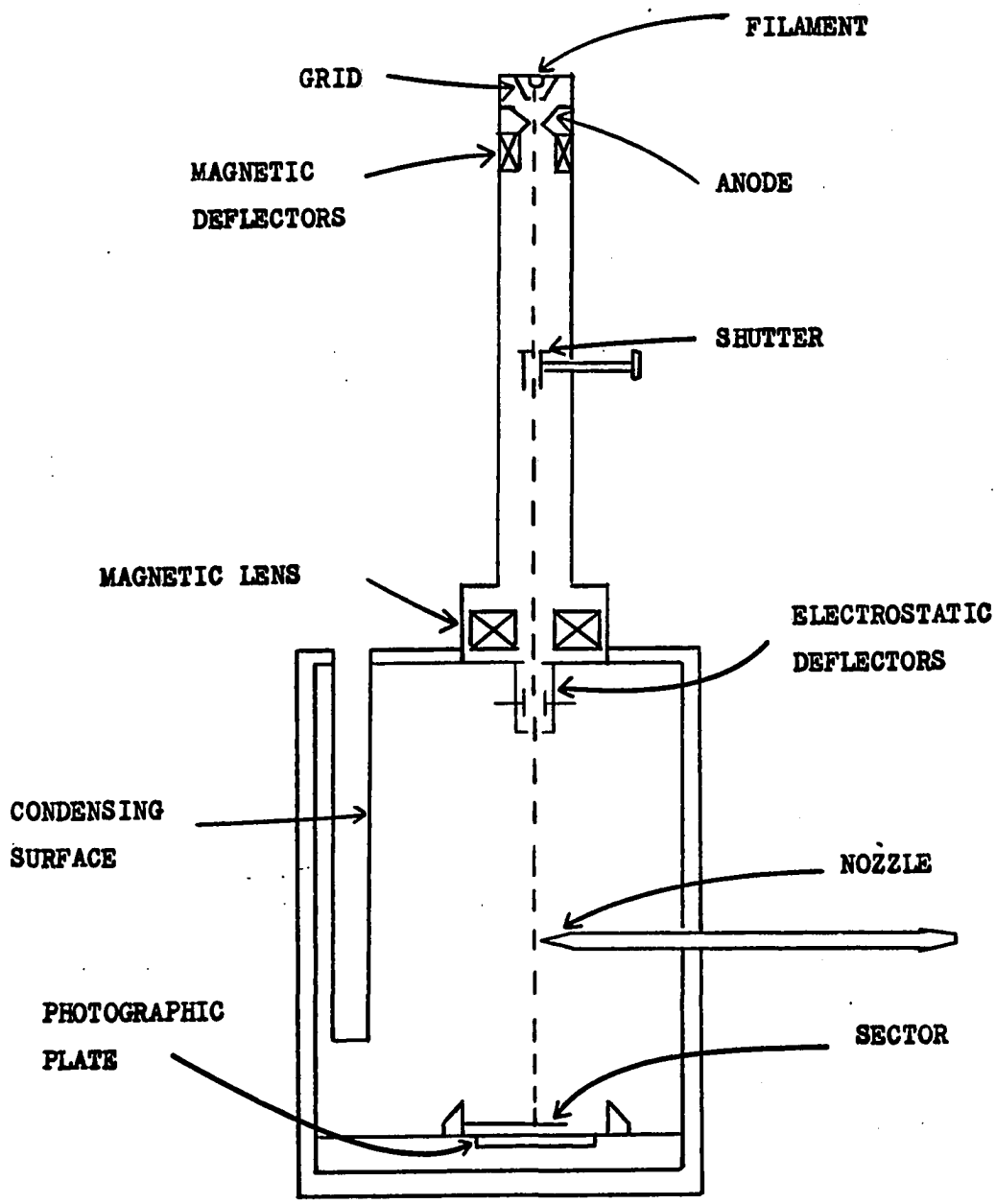

Fig. 13. Schematic diagram showing the essential elements of an electron diffraction apparatus

Table 7. Experimental conditions

Camera Distance	Sector	Sample Temperature	Sample Pressure	Exposure Time	Beam Current
21.089	r^2	-8 °C	1.7 mm.	7 sec.	1.12 μamp
21.051	r^3	20 °C	18 mm.	8 sec.	1.12 μamp
11.084	r^3	20 °C	18 mm.	10 sec.	1.12 μamp

monel system, complete with a nickel nozzle, which could be attached directly to the electron diffraction unit. Due to the high reactivity of the compound, special care was taken in handling the containers and in preparation of the diffraction unit. The customary Television Tube Koat was removed from metal parts of the unit which would have contact with the molecules, and all sections of the monel system were pre-conditioned with ClF_3. The sample was injected into the apparatus as received from Argonne without transfer into other containers.

Sample temperature, pressure, exposure time, and beam current recorded during the course of the experiment are given in Table 7.

Processing of data

Six apparently flawless plates from each of the three different distance-sector combinations were selected for analysis. The diffraction patterns were measured on a modified Sinclair-Smith microphotometer. Phototube voltages were obtained using a voltage-to-frequency converter and a Hewlett-Packard electronic counter-digital recorder. The plates

were spun about their centers during the microphotometering in order to average out emulsion defects. The rotational velocity was adjusted to insure that the plates rotated exactly three revolutions during the one second counting period employed for the reading of each point. Readings were taken at 0.25 mm. intervals while scanning completely across the plate from right to left. Since readings were taken on both sides of the center of rotation for each of six plates, a total of twelve voltage values were used to obtain each experimental intensity point.

Mean absorbancies for each plate A_j were calculated from

$$\bar{A}_j = [(A_R + A_L)/2\ ] - D/4.6$$

where the subscripts R and L refer to data taken to the right and left, respectively, of the center of spin and

$$A_R = \log\ [(V_{100} - V_0^i) / (V_R - V_0^i)],$$

$$A_L = \log\ [(V_{100} - V_0^i) / (V_L - V_0^i)],$$

$$D = (\Delta V - \Delta V_0) / (V_M - V_0^f) + \Delta V_0 / (V_R - V_0^i),$$

$$\Delta V_0 = (V_0^i - V_0^f),$$

$\Delta V = (V_R - V_L)$ for V_R and V_L at the maximum r value.

The V_0^i and V_0^f are the initial and final dark current voltages, V_{100} a clear plate reading, and V the voltage read from the spinning plate. The D term is a correction for drift in the instrument during the recording of data and V_M is V_R at the maximum radial value.

A check for centering error and for random scatter of the readings due to fluctuations in the microphotometer circuits was made on each plate. A plot of the differences between A_R and A_L was made and a set of readings was considered usable if undulations due to centering error were no more than 0.4% and fluctuations due to random scatter were less than 0.1% of the absorbancies.

Relative intensities for each plate were calculated using the relation (90)

$$I_j(s) = \bar{A}_j(1 + \alpha \bar{A}_j)$$

where α was taken as 0.1. The average leveled intensity $I_o(s)$ was calculated from

$$I_o(s) = \sum_{j=1}^{6} I_j^o(s)E_j /6$$

where E_j represents an exposure correction to put all plates on the same basis, and $I_j^o(s)$ denotes the leveled experimental intensity from the j^{th} plate. The $I_j^o(s)$ were obtained from (91)

$$I_j^o(s) = K[I_j(s) - I_{ext}(s)] \, [\phi_{sc}(r)/r^n](\sec^3\phi)/I_{at}$$

where r is the radial coordinate of the photographic plate, ϕ is the scattering angle, and $\phi_{sc}(r)$ is a sector correction function. The constant n is two for data taken using the r^2-sector and three for data taken using the r^3-sector. The $I_j(s)$ are relative intensity values recorded by the

plate and $I_{ext}(s)$ are extraneous intensity values recorded under conditions identical to experimental conditions except that no sample was being passed through the nozzle.

Correction functions $\phi_{sc}(r)$ for the sectors made use of comparisons of experimentally observed and theoretically calculated intensities for monatomic gases. Scattered intensities from argon were blended with readings from an optical comparator to calibrate the r^3-sector. Data from both neon and xenon were used to calibrate the r^2-sector. For the r^2-sector, the calibration curve $\phi_{Xe}(r)$ derived from xenon data, $Z = 54$, differed appreciably at small r from the calibration curve $\phi_{Ne}(r)$ derived from neon data, $Z = 10$. The reason for the discrepancy is probably a breakdown of the energy approximations used to obtain Equation 36. For the xenon atom, the energy differences between bound states of the atom are not small compared to 40,000 electron-volts. In order to compensate both for imperfections in the sector and inaccurate atomic scattering factors for xenon, a sector calibration curve for use in the analysis of XeF_6 data was constructed from a weighted average of neon and xenon calibration curves. The weighting was made according to the formula

$$\phi_{sc}(r) = [\, I_{at}^{Xe} + 6\, I_{at}^{F} \,]/[\, I_{at}^{Xe}/\phi_{Xe}(r) + 6\, I_{at}^{F}/\phi_{Ne}(r) \,],$$

where I_{at}^{Xe} and I_{at}^{F} are theoretical atomic intensities for scattering from xenon and fluorine atoms, respectively.

Analytical functions approximating $F_i(s)$ and $S_i(s)$ were used to calculate the elastic and inelastic scattering factors at arbitrary

Table 8. Parameters used for calculating elastic scattering factors for xenon and fluorine

atom	a_i	b_i	l_i
F	2.00	.00098	2
	-7.00	.0133	3
	14.00	.0115	4
	-1.00	.0773	8
	1.00	.0124	15
Xe	-2.16	.0000098	2
	0.85	-.000032	3
	10.13	.000078	4
	-34.62	.000489	4
	-56.45	.000410	5
	48.32	.000391	6
	36.36	.000406	4
	-42.99	.000536	5
	87.96	.000553	6
	-16.65	.001219	6
	-78.47	.001413	7
	66.60	.001456	8
	40.60	.004108	6
	-10.64	.004221	7
	-6.71	.004834	8
	61.15	.03299	8
	-106.51	.02718	9
	57.23	.02128	10

s values. A function of the form

$$F_i(s) = \sum_j a_j / (1 + b_j s^2)^{l_j}$$

was used to approximate the elastic scattering factors (39, 92). Numerical parameters for $F_i(s)$ are listed in Table 8. The Heisenberg-Bewilogua (33, 34) approximation was used to calculate $S_i(s)$ values.

Experimental reduced intensity data $M(s)_{exp}$ were obtained from the leveled intensity by dividing $I_o(s)$ by an experimental background function $I_B(s)$. If theory and experiment were perfect, $I_B(s)$ would be a constant for all s values. Since in practice these conditions are never fully satisfied, a smooth curve was selected to represent $I_B(s)$ and the intensity curve divided by this background function to obtain $M(s)_{exp}$, or

$$M(s)_{exp} = [I_o(s)/I_B(s)] - 1.$$

Intensity curve analysis

The intensity curve method of analysis (93) attempts to establish simultaneously the background intensity and the molecular distance and amplitude parameters. The weighted sum over experimental points

$$\sum_i w_i [I_o(s)_{calc} - I_o(s)]_i^2$$

is minimized with respect to variation of both molecular parameters and background coefficients. The calculated intensity is given by

$$I_o(s)_{calc} = I_B(s)[\, 1 + R\, M_{th}(s)\,],$$

where R is the index of resolution, and $I_B(s)$ is an analytical background function of the form

$$I_B(s) = \sum_{i=0}^{n} a_i s^i + a_{n+1} \exp(-\alpha s).$$

Expansion constants for this background function are calculated employing a least-squares technique to minimize the difference between a correlation background, $I_b(s)$, where

$$I_b(s) = I_o(s) / [\ 1 + R\ M_{th}(s)\ ],$$

and the background intensity function $I_B(s)$.

Estimates of the internuclear distances and amplitudes of vibration are used to calculate the initial $M_{th}(s)$. All parameters are allowed to vary independently on each iteration and geometric consistancy is not an imposed constraint.

Radial distribution curve analysis

The radial distribution curve method of analysis employs the Fourier sine transform of the reduced molecular intensity to deduce internuclear distances and amplitudes of vibration. The radial distribution function, f(r), has been defined as (94)

$$f(r) = \int_o^\infty s\ M(s)_{exp}\ \exp(-bs^2)\ (\sin sr)\ ds \qquad (39)$$

where $\exp(-bs^2)$ is called the Degard damping factor (95).

As may be seen from Equation 38, the reduced molecular intensity M(s) includes effects of planetary electron scattering on the molecular intensity in the $U_{ij}(s)$ terms. It is convenient in structural studies to make some correction for this non-nuclear scattering before inversion of the data to facilitate the deduction of internuclear parameters. Plotted

in Figure 14 are $U_{ij}(s)$ functions computed for the two different types of bonds found in the XeF_6 molecule. The limit of $U_{ij}(s)$ as s approaches infinity is unity but the deviation from unity is appreciable at small values of s.

Several different methods have been proposed to compensate for the contribution of the electronic environment to the molecular intensity (91, 94, 96, 97). The approach used in this study was to approximate the $U_{ij}(s)$ functions with Gaussian functions of the form

$$N_{ij}(s) = a_{ij} + b_{ij} \exp(-\beta_{ij} s^2)$$

where a_{ij}, b_{ij}, and β_{ij} are constants. A comparison of $N_{ij}(s)$ and $U_{ij}(s)$ functions is given in Figure 14. A corrected reduced intensity function $M_N(s)$ was defined as

$$M_N(s) = \sum_i \sum_j{}' C_{ij} N_{ij}(s) \exp[-(l_m^2)_{ij} s^2/2] [\cos \Delta n_{ij}] \times [\sin s(r_g(1)_{ij} + \phi(s)_{ij})]/s(r_e)_{ij} \qquad (40)$$

and the Fourier sine transform of this function designated as $f_N(r)$, where

$$f_N(r) = \int_0^\infty s\, M_N(s) \exp(-bs^2) (\sin sr)\, ds.$$

The procedure employed was to correct $M(s)_{exp}$ for effects of non-nuclear scattering by use of a calculated function $\Delta M(s)$, where

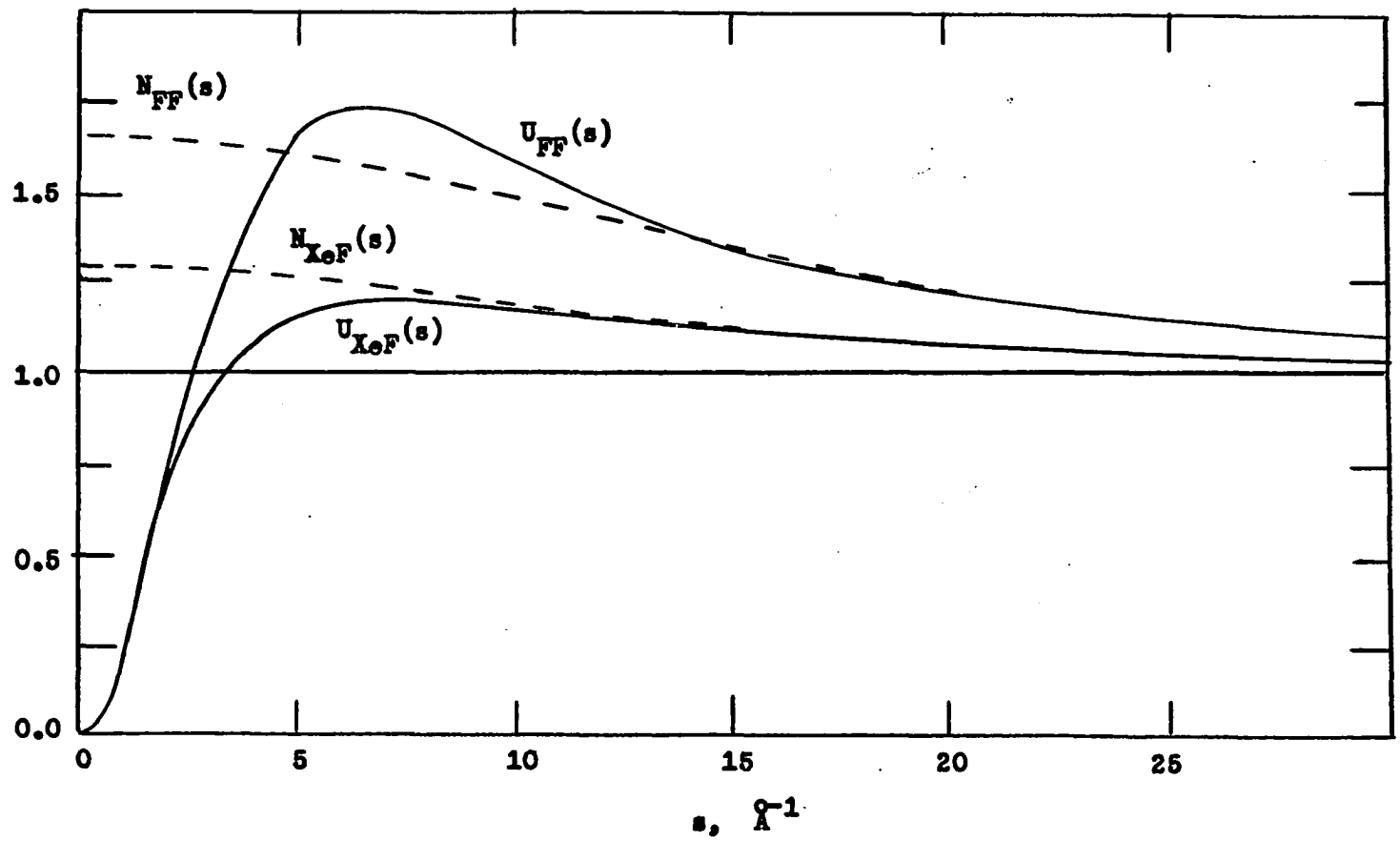

Fig. 14. Solid lines indicate $U_{FF}(s)$ and $U_{XeF}(s)$ functions for fluorine-fluorine and xenon-fluorine bonds, respectively, in the XeF_6 molecule. The dashed curves represent the corresponding analytical approximations $N_{ij}(s)$ to the $U_{ij}(s)$ functions.

$$\Delta M(s) = M_N(s) - M_{th}(s),$$

and then to invert the corrected experimental reduced intensity

$$M_N(s)_{exp} = M(s)_{exp} + \Delta M(s)$$

to obtain $f_N(r)_{exp}$. Experimental data were obtained from $s_{min} = 2.6$ to $s_{max} = 39.1$. Some compensation for lack of data in the ranges $0 < s < s_{min}$ and $s_{max} < s < \infty$ had to be made, therefore, to make possible evaluation of Equation 39. Theoretical $M_N(s)$ values were used in the region $s = 0$ to $s = s_{min}$ and an integral termination correction (98) was applied to make allowance for lack of data from $s = s_{max}$ to $s = \infty$. Curves were calculated from

$$f_N(r)_{exp} = \sum_{s=0}^{s_{min}} s\, M_N(s)\, \exp(-bs^2)(\sin sr)\, \Delta s + \sum_{s=s_{min}}^{s_{max}} s\, M_N(s)_{exp}\, \exp(-bs^2)(\sin sr)\, \Delta s + I_{term}$$

where I_{term} represents a correction for integral termination (98). The background intensity function was determined using the criterion of a non-negative radial distribution curve. A smooth curve $I_B(s)$ was drawn through $I_o(s)$ and was adjusted to eliminate negative regions in $f_N(r)_{exp}$.

Use of theoretical reduced intensity values in the region $s = 0$ to $s = s_{min}$ and in calculation of $\Delta M(s)$ causes the radial distribution curve to be somewhat dependent on the parameters of a theoretical model. The principal advantage of $M_N(s)$ functions is that the $f_N(r)_{exp}$ curve generated utilizing these functions is not too sensitive to the input

parameters. The method of correcting for non-nuclear scattering formerly used in this research group (88, 91) employed a "constant coefficient" reduced intensity function $M_c(s)$ instead of the $M_N(s)$ function. The $M_c(s)$ functions are analogous to $M_N(s)$ functions and are defined according to Equation 40 but with the $N_{ij}(s)$ taken as unity. Use of the "constant coefficient" method with XeF_6 data produced radial distribution curves which were very sensitive to the input parameters. When the $M_N(s)$ basis was utilized, however, the sensitivity to input parameters was almost totally eliminated.

Molecular parameters were obtained from $f_N(r)_{exp}$ curves by means of a least-squares program due to Boates (99). In this program, the function

$$\Delta = \sum_i \left[f_N(r) - f_N(r)_{exp} \right]_i^2$$

is minimized by use of the Gauss-Newton method for least squares. The expressions used to calculate $f_N(r)$ are those of Kuchitsu and Bartell (87) with corrections made for failure of the Born approximation (82, 100).

A symmetry is assumed for the molecule and all internuclear distance parameters r_g are calculated relative to this symmetry. Geometric consistancy is maintained in each iteration by allowing only independent parameters to vary and recalculating all dependent parameters each cycle. Corrections for "shrinkage effects" (101, 102, 103) in the nonbonded distances may also be included.

Errors

Uncertainties in structural parameters derived from electron diffraction data may result from either theoretical or experimental deficiencies.

The theoretical expressions employed assume that the energy of incident electrons is extremely large compared to molecular energy levels, that molecular electron densities are the sum of spherical atomic densities, and that effects of polarization and multiple scattering are negligible. Recent calculations of Bonham (61, 64, 68, 104, 105) indicate that these assumptions provide reasonable approximations, especially for molecules containing atoms of low atomic number. For molecules containing atoms of atomic number thirty or higher, deviations due to the failure of the energy approximations become important. The present correction for failure of the Born approximation, for example, is only an approximation. For bonds with large differences in atomic number, a mean uncertainty of about 5% in this correction is probable and this error causes relatively large uncertainties in amplitudes of vibration and in resolution of component distances in a composite f(r) peak, as will be discussed later.

Experimental errors may be of three different types: (a) measurement of scattering angle and determination of electronic wavelength gives rise to systematic errors which affect primarily the bond lengths and secondarily the amplitudes; (b) inaccurate emulsion calibration and improper extraneous intensity corrections cause systematic errors affecting the amplitudes of vibration and, possibly, the bond lengths; (c) random errors in the sector calibration curves and random errors due to fluctuations in microphotometer readings and emulsion irregularities

contribute to uncertainties in both interatomic distances and amplitudes of vibration. These errors do not exhaust all possible sources but are thought to include the primary contributors in this experiment.

Uncertainties in the parameters were estimated during the least-squares analyses employing the technique of Whittaker and Robinson (108). All errors reported are uncertainties in independent parameters relative to the assumed symmetry of the molecule. No estimates of error were calculated relaxing the imposed symmetry conditions and the error inherent in drawing the background function was not included.

Molecular Parameters of XeF_6

Data were analysed using primarily the radial distribution curve method. At various times during the analysis, models were tested employing the total intensity curve method to insure that convergence in r space also implied convergence in s space. More extensive use of the intensity curve analysis was not feasible because of the lack of geometric constraints in the available least-squares program.

Plotted in Figures 15, 16, and 17 are the experimental intensity and background intensity values for data taken at the long and middle distances and for data obtained with the r^2-sector.

Plotted in Figure 18 is a synthetic $f_N(r)$ function calculated for an XeF_6 model with O_h symmetry. For comparison is shown an experimental $f_N(r)_{exp}$ curve in which the input parameters for $M_N(s)$ below s_{min} are the same as the O_h input parameters for the synthetic curve. The discrepancy between calculated and experimental curves is apparent. The peak at about 1.9 Å in the experimental curve due to the Xe-F distance is clearly

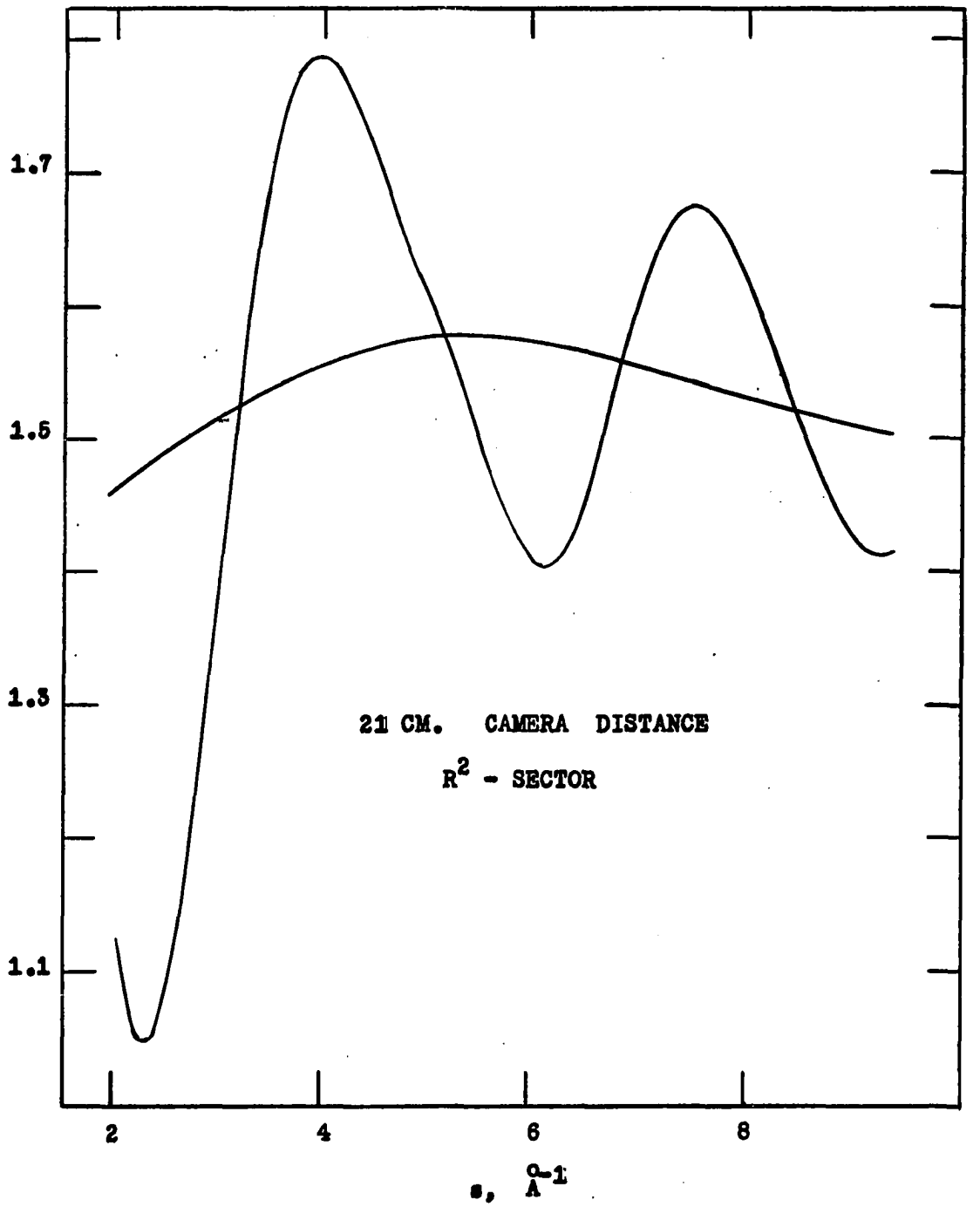

Fig. 15. Plots of $I_o(s)$ and $I_B(s)$ for the 21 cm. camera distance using the r^2-sector

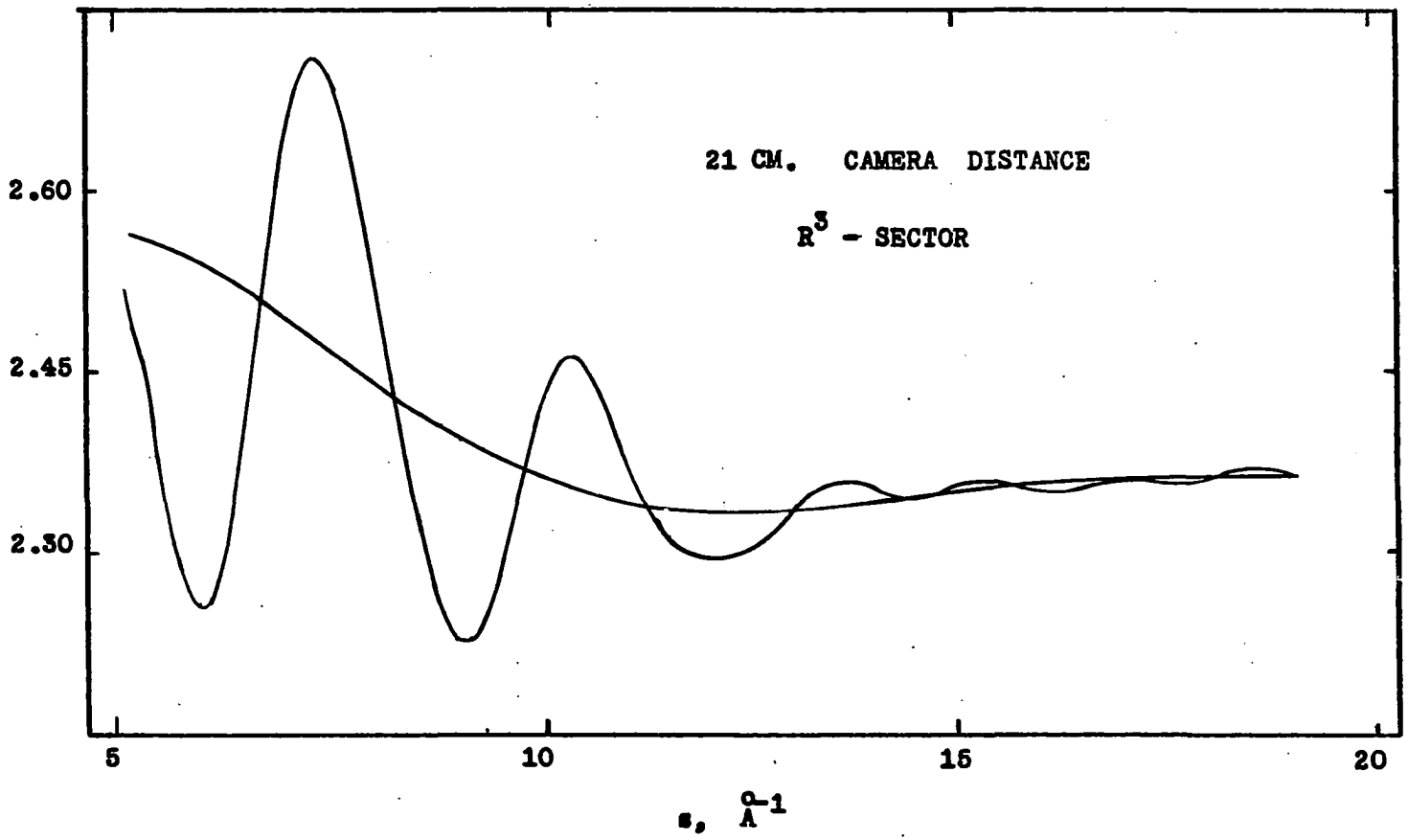

Fig. 16. Plots of $I_o(s)$ and $I_B(s)$ for the 21 cm. camera distance using the r^3-sector

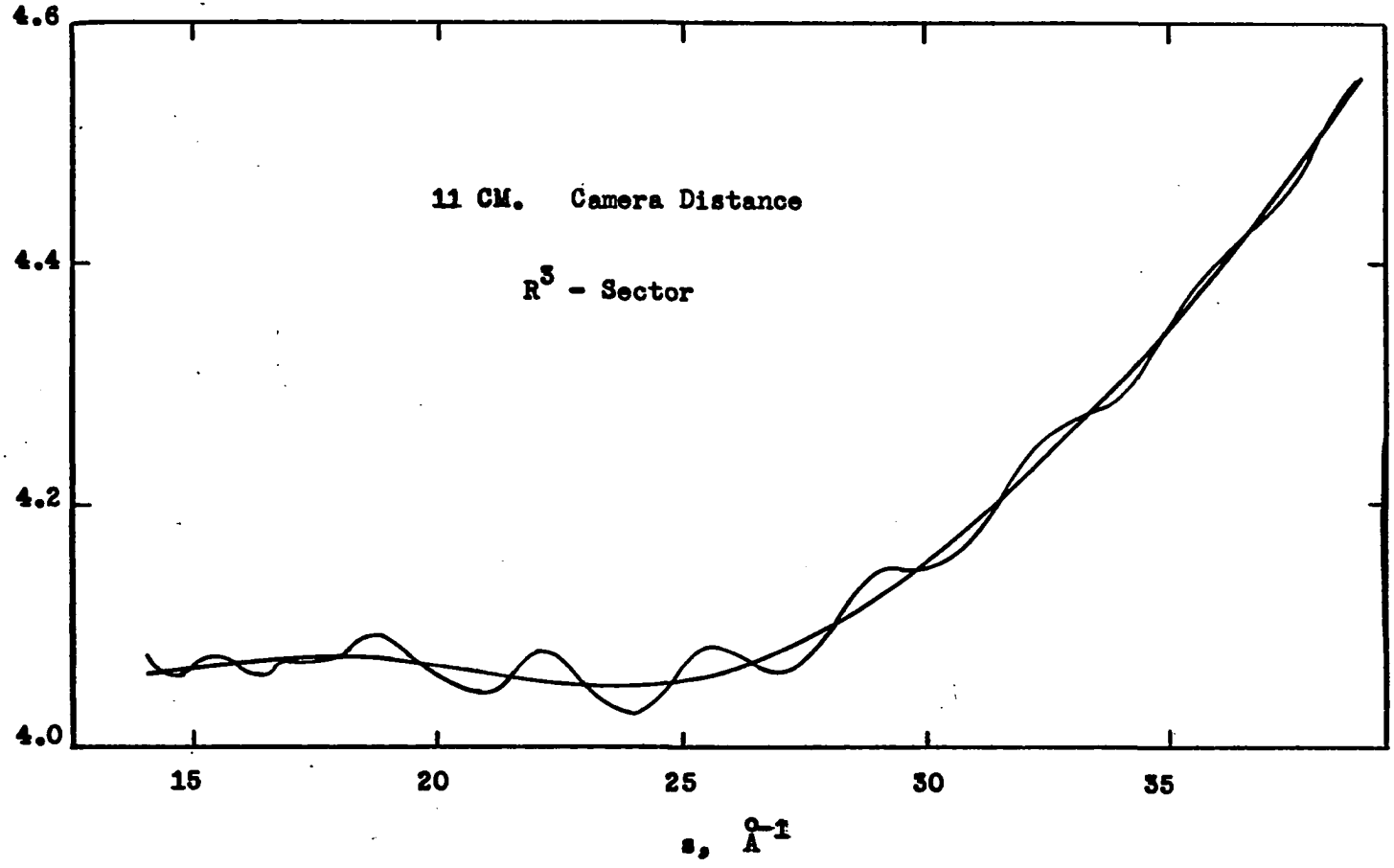

Fig. 17. Plots of $I_o(s)$ and $I_B(s)$ for the 11 cm. camera distance using the r^3-sector

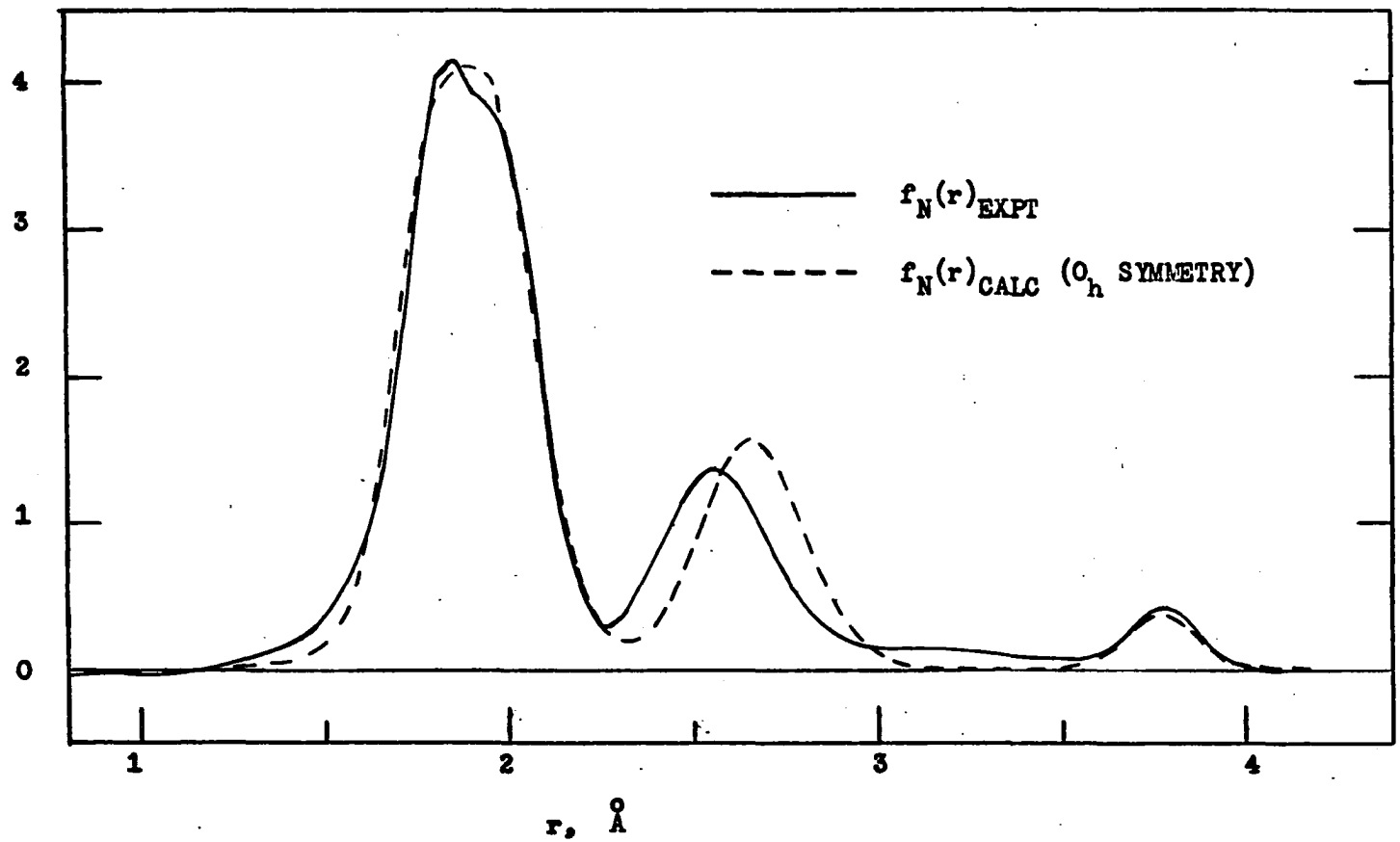

Fig. 18. The dashed curve represents a synthetic $f_N(r)$ function calculated for an XeF_6 model with O_h symmetry. An experimental $f_N(r)$ curve in which input parameters for $M_N(s)$ below s_{min} are the same as the O_h input parameters is shown as a solid curve.

asymmetric. This asymmetry implies that the xenon-fluorine bonds are not all of the same length. In addition, the experimental peak due to the intermediate range fluorine-fluorine distances is shifted to a considerably shorter mean distance than the $\sqrt{2}\, r_{XeF}$ value required by O_h symmetry. It is obvious that the xenon hexafluoride molecule is not a regular octahedron.

The shape of the Xe-F peak is determined not only by amplitudes of vibration and distance splits of the component bonds but also by the Born phase shift Δn_{XeF}. The approximation usually employed to calculate values of Δn_{ij} is based on the Thomas-Fermi model for the atomic potential (84). This basis is known to provide inaccurate values of the phase shift n_i for interaction with a single atom i but is thought to give reasonably accurate differences in phase Δn_{ij} for a bond between atoms i and j. Recent results of Schomaker, et al. (107), however, indicate that the Δn_{ij} calculated from the Thomas-Fermi model may be in error by as much as 10% for bonds with large differences in atomic number.

The value of s where Δn_{ij} is equal to $\pi/2$ can be estimated from the experimental intensity curves. A visual inspection of the intensity curves indicates that this "cutoff value", s_c, is about 17.0 Å^{-1}, whereas the calculated value (84) is 18.7 Å^{-1}. Calculations were performed to establish an experimental value of s_c because of the discrepancy between calculated and experimental values. When bond lengths, bond angles, and amplitudes of vibration were allowed to adjust for a given s_c, however, intensity curve and radial distribution curve analyses both obtained comparable total standard deviations for any value of s_c in the range

$16.0 < s_c < 17.5$. Therefore, a value of $s_c = 16.6$ Å^{-1} was arbitrarily assumed for all further calculations.

Three slightly different geometric models were found to be effective in fitting the experimental data. In each case the number of non-equivalent Xe-F bond lengths was limited to two. Three different amplitudes of vibration were employed for nonbonded F...F distances but only two, l_1 and l_2, were allowed to vary. The third, l_3, was taken as $l_1 + 0.035$ for models A and B, and $l_1 + 0.185$ for model C.

A drawing of model A is given in Figure 19. The molecule possesses C_{2v} symmetry and the following restrictions were assumed:

(a) atoms F_1, F_3, F_4, F_6, and Xe are coplanar and the associated Xe-F bond lengths are equal,

(b) the angles $\angle F_1XeF_6$, $\angle F_4XeF_6$, and $\angle F_5XeF_4$ are equal,

(c) atoms F_2, F_5, and Xe form a plane perpendicular to the $F_1F_3F_4$-plane and bisecting $\angle F_1XeF_3$, and

(d) Xe-F bonds to F_2 and F_5 are of equal length and are bent β degrees off the axis.

Model B was identical to model A except that the symmetry was reduced to C_s by constraining the Xe-F_5 bond to the axis and allowing the Xe-F_2 bond to bend β' degrees off the axis.

Model C was an octahedron with one face opened such that the molecule maintained C_{3v} symmetry. A projection of the model on a plane perpendicular to the three-fold symmetry axis is shown in Figure 20. Bonds to atoms F_1, F_2, and F_3 were longer than the mean Xe-F length and those to F_4, F_5, and F_6 shorter. The angle between the symmetry axis and the

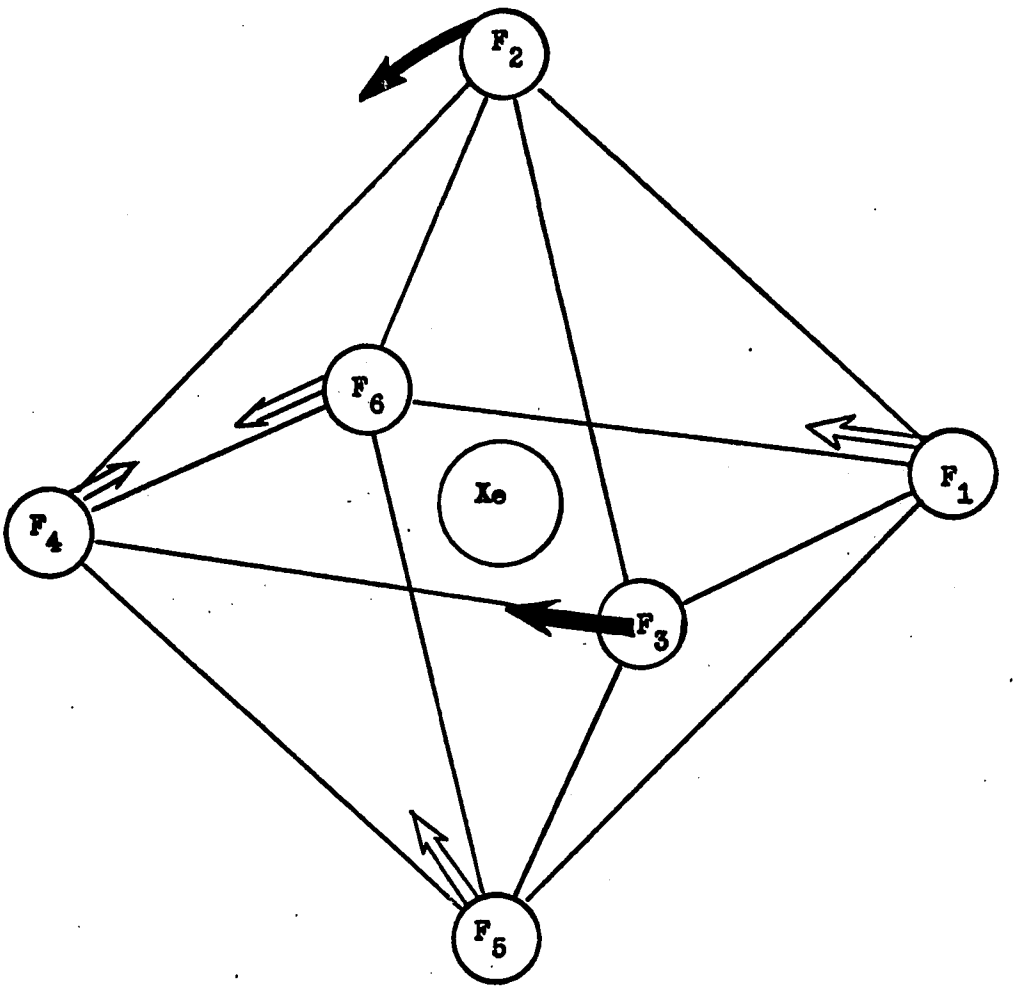

Fig. 19. A drawing representing the distortion from O_h symmetry found in model A

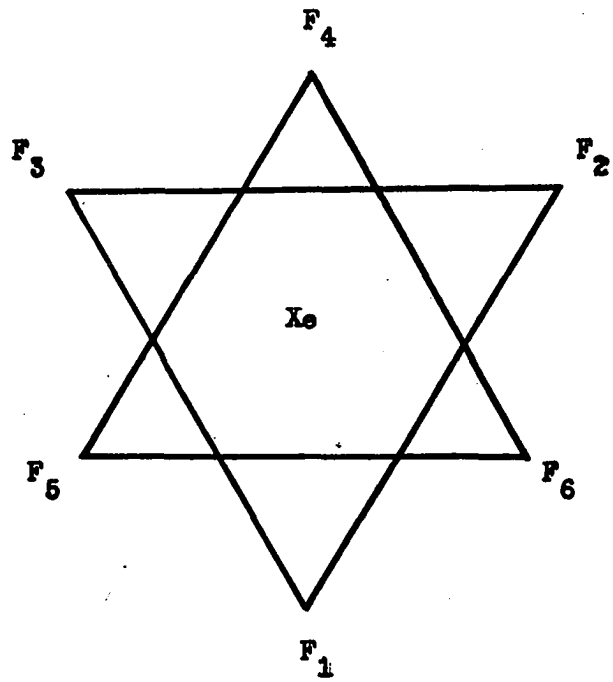

Fig. 20. Drawing of model C projected on a plane perpendicular to the three-fold symmetry axis

and the Xe-F_1 bond is designated δ and that between the symmetry axis and the Xe-F_4 bond, γ .

Independent parameters, standard errors relative to assumed symmetries, and internuclear distances for models A, B, and C are given in Table 9. Shrinkage corrections $\int r$ are estimates made from shrinkage values calculated for octahedral molecules by Meisingeth and Cyvin (108). The estimates are rough indeed since the amplitudes of XeF_6 vibrations are quite different from those of the comparison compounds, and the symmetry is lower.

A modification of model A in which Xe-F bonds to F_1, F_2, F_3, and F_5

Table 9. Independent parameters, internuclear distances r_g, amplitudes of vibration l, and bond multiplicities M for models A, B, and C

distance	$r_g(0)$	δr	l	M	
Model A		Symmetry C_{2v}			σ_{tot} = 0.0471
Xe - F_5	1.831	0.000	0.082	2	r_{XeF} = 1.886 ± 0.005
Xe - F_1	1.914	0.000	0.062	4	
$F_1 \cdots F_6$	2.506	0.003	0.098	3	Δr_{XeF} = 0.083 ± 0.015
$F_2 \cdots F_6$	2.557	0.002	0.098	4	$\angle F_1XeF_6$ = 81.90° ± 0.28°
$F_2 \cdots F_3$	2.708	0.002	0.133	4	β = 5.02° ± 0.36°
$F_1 \cdots F_3$	3.212	0.003	0.133	1	
$F_2 \cdots F_5$	3.644	0.003	0.052	1	
$F_1 \cdots F_4$	3.787	0.003	0.052	2	
Model B		Symmetry C_s			σ_{tot} = 0.0470
Xe - F_5	1.825	0.000	0.079	2	r_{XeF} = 1.886 ± 0.005
Xe - F_1	1.916	0.000	0.059	4	
$F_1 \cdots F_6$	2.500	0.003	0.093	3	Δr_{XeF} = 0.0907 ± 0.015
$F_2 \cdots F_6$	2.516	0.002	0.093	2	$\angle F_1XeF_6$ = 81.60° ± 0.28°
$F_5 \cdots F_6$	2.644	0.002	0.093	2	β' = 7.14° ± 0.62°
$F_3 \cdots F_5$	2.644	0.002	0.128	2	
$F_1 \cdots F_2$	2.730	0.002	0.128	2	
$F_1 \cdots F_3$	3.232	0.003	0.128	1	
$F_2 \cdots F_5$	3.640	0.003	0.052	1	
$F_1 \cdots F_4$	3.787	0.003	0.052	2	
Model C		Symmetry C_{3v}			σ_{tot} = 0.0503
Xe - F_1	1.912	0.000	0.065	3	r_{XeF} = 1.887 ± 0.005
Xe - F_4	1.862	0.000	0.085	3	
$F_1 \cdots F_5$	2.523	0.002	0.092	6	Δr_{XeF} = 0.050 ± 0.015
$F_4 \cdots F_5$	2.652	0.003	0.092	3	γ = 124.61° ± 0.24°
$F_1 \cdots F_2$	2.939	0.003	0.277	3	δ = 62.66° ± 0.23°
$F_1 \cdots F_4$	3.765	0.003	0.070	3	

were longer than the mean length was investigated. The fit of the radial distribution curve with this model was inferior to that obtained with model A. The distribution of Xe-F bond lengths in the molecule was not uniquely determined but, when only two different Xe-F bond lengths were employed in models A and B, the best fit of the experimental data was obtained with all equatorial bonds longer than the mean distance. If models A or B are the correct models, it is likely that three or more nonequivalent bond lengths exist. Evaluation of structural details of this sort, however, would be beyond the accuracy of the present experimental data.

Linear combinations of the triply degenerate F_{1g} and F_{1u} vibrational modes (109) of an octahedral molecule produce distortions from O_h symmetry similar to the distortions found in models A and C. If F_{1g} and F_{1u} denote the sum of the three components of the normal vibrations, the distortion of model A is closely approximated by the vibration $F_{1g} + F_{1u}$, and that of model C by $F_{1g} - F_{1u}$. The possibility was investigated that the distortion from O_h symmetry observed in the radial distribution curve was the result of unusually large amplitudes of vibration along some symmetry coordinate about an equilibrium O_h configuration. Radial distribution curves were constructed to represent a molecule with O_h symmetry undergoing large vibrations. The components of f(r) were taken to be f(r) curves with 0% (O_h symmetry), 33%, 66%, 100% (model C), 133%, and 200% of the distortion from O_h symmetry to model C. A weighted sum based on the assumption of a Gaussian distribution of models about an octahedral structure was used to simulate the f(r) curve. The weightings used in this sum are shown in

Figure 21 (a). A least-squares computer program was then employed to deduce the weighting associated with the smallest root-mean-square deviation between experimental and calculated f(r) curves. The weighting associated with the best fit is shown in Figure 21 (b). A comparison of the root-mean-square deviations given in Figure 21 clearly indicates that the best fit of the experimental data is not with a molecule undergoing extremely large vibrations about an equilibrium O_h configuration.

Discussion

The mean Xe-F bond length of $r_g = 1.886 \pm 0.005$ Å for the hexafluoride is consistent with the trend set by XeF_4, $r = 1.953 \pm 0.002$ Å (21), and XeF_2, $r = 2.00 \pm 0.01$ Å (20). The Xe-F vibrational amplitudes, however, appear to be larger than those found for the related molecule TeF_6, where $l_{TeF} = 0.039$ $Å^{-1}$ (108), and the difference in amplitudes for the two Xe-F bonds is opposite in sign from what one would predict from a simple extension of Badger's rule (110, 111, 112).

The error in the correction for failure of the Born approximation produces a corresponding error in both l_{XeF} and the split Δr_{XeF} of xenon-fluorine distances. Calculations indicated that the uncertainty in s_c was ± 0.8 $Å^{-1}$, and that this uncertainty alone causes an uncertainty of ± 0.015 Å in l_{XeF}. If the errors due to the assumption of only two different Xe-F bond lengths and to the level of noise in $f_N(r)_{exp}$ near the Xe-F peak are taken into account, the accumulative uncertainty in the mean of the two Xe-F amplitudes is probably 0.020 Å. The error in Δr_{XeF} was not as easy to estimate because its value is determined both by the shape of the Xe-F peak and by the distribution of nonbonded distances. A

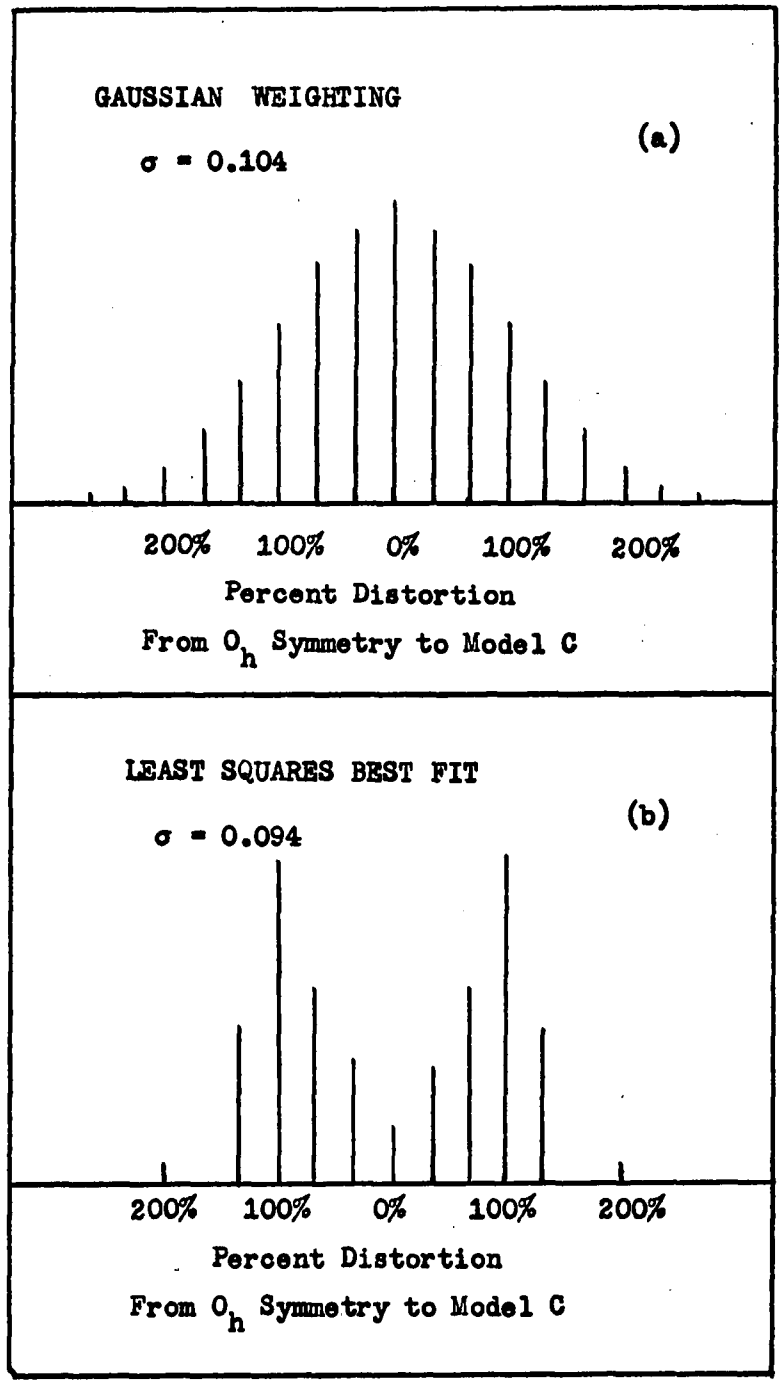

Fig. 21. Weightings for f(r) curves constructed from models with different percent distortion from O_h symmetry to model C. (a) Weighting for a Gaussian distribution of models about O_h symmetry. (b) Weighting associated with smallest root mean square deviation from experimental f(r)

reasonable estimate of the uncertainty in Δr_{XeF} is ± 0.015 Å.

The most significant conclusion of this investigation is that XeF_6 does not possess octahedral symmetry. This conclusion is based both on the shape of the Xe-F peak and on the distribution of F...F nonbonded distances implied by the radial distribution curve. In any electron diffraction study the number of independent parameters which may be effectively solved for is limited by the number of distinct features appearing in the f(r) curve. Because of this limitation and the unfavorable ratio of atomic numbers in XeF_6, a unique structure for the molecule was not established. It was possible, however, to eliminate the possibility that the molecule possessed O_h symmetry and to deduce general characteristics of the structure. An investigation of models A, B, and C shows that the differences in bond angles are only a matter of a few degrees and that the nature of the distortion from O_h symmetry is much the same in all models. The fluorines on one side of the molecule are pushed apart and this deformation compresses the fluorines toward the other side of the molecule.

The structures of XeF_2 and XeF_4 were correctly predicted by several authors employing molecular orbital approaches (28, 30, 113, 114, 115). Extension of these approaches to XeF_6, however, resulted in predictions of octahedral symmetry. The deficiency of these approaches in the XeF_6 case was apparently an inaccurate description of the role of the xenon 5s and 4d orbitals in the bonding scheme. On the basis of energy and orbital overlap considerations, mixing of Xe(5s) and Xe(4d) orbitals and the XeF_6 molecular orbitals was thought to be very small (30, 115) and a

distortion from O_h symmetry was considered to be unlikely. On the other hand, preliminary calculations of Bartell[2] indicate that even if simple molecular orbital theory does not unambiguously give the equilibrium structure, it does demonstrate that deformations from O_h symmetry of the observed form are much less costly energetically than deformations of arbitrary form.

One theoretical model, the valence-shell electron-pair repulsion model of Gillespie and Nyholm (27, 116, 117), deserves special note. The approximate mean Xe-F bond length, a distortion from O_h symmetry, and the existence of nonequivalent Xe-F bond lengths were predicted from the postulates of this model. The only thing not correctly predicted was the effective size of the lone pair of electrons, for the observed deviation from O_h symmetry was significantly smaller than the predicted deviation. Gillespie and Nyholm propose that lone pairs of electrons occupy a larger volume in the valence shell than a bonding pair. In models A and B the equatorial F-Xe-F bond angles are deformed only about half way from those of a square array to those of a regular pentagon, although the axial fluorines are bent away from the lone pair rather than from the equatorial fluorines. In model C the gap in the opened octahedral face is smaller than a fluorine atom.

Studies have established that ions such as $[TeCl_6^{-2}]$ (118, 119),

---

[2]Bartell, L. S., Department of Chemistry, University of Michigan, Ann Arbor, Michigan, A molecular orbital study of XeF_6. Private communication. 1966.

$[TeBr_6^{-2}]$ (120), and $[SbBr_6^{-3}]$ [3] which are isoelectronic with XeF_6 possess O_h symmetry, whereas the present study indicates that XeF_6 does not. The simple scheme predicting stereochemistry on the basis of the number of valence-shell electron pairs is not as successful for coordination number seven as it is for lower coordination numbers. Perhaps one reason for this lies in the following point made by Gillespie (121). For lower coordination the stereochemistry is insensitive to the form assumed for the interaction potential, but, at coordination seven or higher, the equilibrium geometry depends critically on the form of the potential.

---

[3] Lawton, S. and Jacobson, R., Department of Chemistry, Iowa State University of Science and Technology, Ames, Iowa, The crystal structure of $(NH_4)_4Sb_2Br_{12}$. Private communication. 1965.

SUMMARY

The theory of x-ray diffraction by gas atoms is examined from the standpoint of one-electron and two-electron operators. Elastic scattering depends on one-electron operators and, hence, may be used to determine the density of electrons about nuclei, a one-electron property. On the other hand, it is found that inelastic scattering by atoms possessing more than one electron depends on the distribution of distances between electrons. Consequently, the mean density of electrons about other electrons, an important two-electron property, can also be determined from diffraction experiments.

Electron-electron and electron-nuclear radial distribution functions $P(r_{ij})$ and $D(r_i)$ are calculated for the ground states of helium-like systems ($Z = 2$ to 8) and the ground state of the beryllium atom. Computations were based on correlated and uncorrelated wavefunctions. Elastic and inelastic scattering factors for calculating the intensities $I(\phi)$ of x rays scattered by these systems were determined from the distribution functions. Correction functions $\Delta P(r_{12})$ and $\Delta I(\phi)$ representing the differences between correlated and uncorrelated results were found to follow a simple dependency on atomic number for the helium-like systems. A scheme to predict correlation effects in many electron atoms was derived from this simple dependency. Correlation shifts in $P(r_{ij})$ and $I(\phi)$ for the beryllium atom were computed and compared to shifts predicted employing the simple scheme. Agreement between predicted and calculated shifts was good.

Radial distribution functions $P(r_{ij})$ for neon and argon atoms were derived from Laurila's experimental x-ray intensities. The resulting

distribution functions were used to calculate experimental electron-electron potential energy values, V_{ij}. The V_{ij} for neon and argon calculated from the analytical fits of the experimental data are 1.12 a.u. and 1.40 a.u., respectively. Corresponding values of 1.20 a.u. and 1.36 a.u. were calculated from self consistent field wavefunctions. The $P(r_{ij})$ functions compared favorably with those calculated from existing wavefunctions. Uncertainties in the distribution functions due to the scatter of experimental data points and to the restricted angular range of the data were large enough to obscure effects of electron correlation.

Xenon hexafluoride was studied to determine its molecular geometry and to test various theories on chemical bonding. The results of the study indicate that the molecule exists as a distorted octahedron with non-equivalent xenon-fluorine bond lengths. None of the currently popular theories on bonding and steriochemistry predicted the exact geometry but one, due to Gillispie and Nyholm, did correctly predict some important structural features.

LITERATURE CITED

1. Debye, P., Annalen der Physik 46, 809 (1915).

2. Waller, I. and Hartree, D. R., Proceedings of the Royal Society (London) A124, 119 (1929).

3. Barrett, C. S., Physical Review 32, 22 (1928).

4. Herzog, G., Zeitschrift fuer Physik 69, 207 (1931).

5. Wollan, E. O., Physical Review 35, 862 (1930).

6. Herzog, G., Zeitschrift fuer Physik 70, 583 (1931).

7. Wollan, E. O., Physical Review 38, 15 (1931).

8. Compton, A. H., Physical Review 35, 925 (1930).

9. Slivnik, J., Brcic, B., Volavsek, B., Marsel, J., Vrscay, V., Smlac, A., Frlec, B. and Zemljic, Z., Croatica Chemica Acta 34, 253 (1962).

10. Malm, J. G., Sheft, I. and Chernick, C. L., Journal of the American Chemical Society 85, 110 (1963).

11. Weaver, E. E., Weinstock, B. and Knop, C. P., Journal of the American Chemical Society 85, 111 (1963).

12. Dudley, F. B., Gard, G. and Cady, G. H., Inorganic Chemistry 2, 228 (1963).

13. Claassen, H. H., Selig, H. and Malm, J. G., Journal of the American Chemical Society 84, 3593 (1962).

14. Chernick, C. L., Science 138, 136 (1962).

15. Weeks, J. L., Chernick, C. L. and Matheson, M. S., Journal of the American Chemical Society 84, 4612 (1962).

16. Hoppe, R., Dahne, W., Mattauch, H. and Rodder, K. M., Angewandte Chemie, International Edition in English 1, 599 (1962).

17. Smith, D. F., Journal of Chemical Physics 38, 270 (1963).

18. Studier, M. H. and Sloth, E. N., Journal of Physical Chemistry 67, 925 (1963).

19. Seigel, S. and Gebert, E., Journal of the American Chemical Society 85, 240 (1963).

20. Levy, H. A. and Agron, P. A., Journal of the American Chemical Society 85, 241 (1963).

21. Bohn, R. K., Katada, K., Martinez, J. V. and Bauer, S. H. An electron-diffraction study of gaseous xenon tetrafluoride. In Hyman, Herbert H., editor. Noble-gas compounds. p. 238. Chicago, Illinois, University of Chicago Press. 1963.

22. Ibers, J. A. and Hamilton, W. C., Science 139, 106 (1963).

23. Templeton, D. H., Zalhin, A., Forester, J. D. and Williamson, S. M., Journal of the American Chemical Society 85, 242 (1963).

24. Burns, J. H., Agron, P. A. and Levy, H. A., Science 139, 1209 (1965).

25. Smith, D. F. Information on bonding in xenon compounds from infrared spectra. In Hyman, Herbert H., editor. Noble-gas compounds. p. 295. Chicago, Illinois, University of Chicago Press. 1963.

26. Bohn, R. K., Dissertation Abstracts 25, 3282 (1964).

27. Gillespie, R. J. The noble-gas fluorides, oxyfluorides, and oxides: predictions of molecular shapes and bond lenghts. In Hyman, Herbert H., editor. Noble-gas compounds. p. 333. Chicago, Illinois, University of Chicago Press. 1963.

28. Coulson, C. A., Journal of the Chemical Society (London) 1964, 1442.

29. Malm, J. G., Selig, H., Jortner, J. and Rice, S. A., Chemical Reviews 65, 199 (1965).

30. Urch, D. S., Journal of the Chemical Society (London) 1964, 5775.

31. Wentzel, G., Zeitschrift fuer Physik 43, 779 (1927).

32. Klein, O., Zeitschrift fuer Physik 41, 407 (1927).

33. Heisenberg, W., Physikalische Zeitschrift 32, 737 (1931).

34. Bewilogua, L., Physikalische Zeitschrift 32, 740 (1931).

35. Freeman, A. J., Acta Crystallographica 12, 274 (1959).

36. Thomson, J. J. Conduction of electricity through gases. Cambridge, England, Cambridge University Press. 1906.

37. Pirenne, M. H. The diffraction of x-rays and electrons by free molecules. Cambridge, England, Cambridge University Press. 1946.

38. James, R. W. The optical principles of the diffraction of x-rays. London, England, G. Bell and Sons, Limited. 1954.

39. Hauptman, H. and Karle, J., Physical Review 77, 491 (1950).

40. Compton, A. H., Physical Review 22, 409 (1923).

41. Herzog, G., Helvetica Physica Acta 2, 169 (1929).

42. Coulson, C. A. and Neilson, A. H., Proceedings of the Physical Society (London) 78, 831 (1961).

43. Gilbert, T. L., Reviews of Modern Physics 35, 491 (1963).

44. Lester, W. A. and Krauss, M., Journal of Chemical Physics 41, 1407 (1964).

45. Curl, R. F. and Coulson, C. A., Proceedings of the Physical Society (London) 85, 647 (1965).

46. Roothaan, C. C. J., Sachs, L. M. and Weiss, A. W., Reviews of Modern Physics 32, 186 (1960).

47. Roothaan, C. C. J. and Weiss, A. W., Reviews of Modern Physics 32, 194 (1960).

48. Goodisman, J. and Klemperer, W., Journal of Chemical Physics 38, 721 (1963).

49. Karplus, M. and Kolher, H. J., Journal of Chemical Physics 38, 1263 (1963).

50. Møller, C. and Plesset, M. S., Physical Review 46, 618 (1934).

51. Colen, M. and Dalgarno, A., Proceedings of the Physical Society (London) 77, 748 (1961).

52. Boys, S. F., Proceedings of the Royal Society (London) A201, 125 (1950).

53. Freeman, A. J., Acta Crystallographica 12, 929 (1959).

54. Freeman, A. J. and Watson, R. E., Acta Crystallographica 15, 682 (1962).

55. Hylleraas, E. A., Zeitschrift fuer Physik 54, 347 (1929).

56. Slater, J. C., Physical Review 36, 57 (1930).

57. Tuan, D. F. and Sinanoglu, O., Journal of Chemical Physics 41, 2677 (1964).

58. McKoy, V. and Sinanoglu, O., Journal of Chemical Physics 41, 2689 (1964).

59. Clementi, E., Journal of Chemical Physics 38, 2248 (1963).

60. Pekeris, C. L., Physical Review 112, 1649 (1958).

61. Iijima, T., Bonham, R. A. and Ando, T., Journal of Physical Chemistry 67, 1472 (1963).

62. Rutherford, E., Philosophical Magazine 21, 669 (1911).

63. Bartell, L. S. and Gavin, R. M., Journal of the American Chemical Society 86, 3493 (1964).

64. Bonham, R. A. and Iijima, T., Journal of Physical Chemistry 67, 2266 (1963).

65. Compton, A. H. and Allison, S. K. X-rays in theory and experiment. New York, New York, D. Van Nostrand Co., Inc. 1934.

66. Breit, G., Physical Review 27, 262 (1924).

67. Dirac, P. A. M., Proceedings of the Royal Society (London) A111, 405 (1926).

68. Bonham, R. A., Journal of Chemical Physics 43, 1460 (1965).

69. Laurila, E., Annales Academiae Scientiarum Fennicae, Series A, II, 57, 7 (1941).

70. Chipman, D. R. and Jennings, L. D., Physical Review 132, 728 (1963).

71. Freeman, A. J., Acta Crystallographica 12, 261 (1959).

72. Berghius, J., Haanappel, I. M., Potters, M., Loopstra, B. O., MacGillavry, C. H. and Veenendaal, A. L., Acta Crystallographica 8, 478 (1955).

73. Freeman, A. J., Acta Crystallographica 13, 190 (1960).

74. Allen, J. C., Journal of Chemical Physics 34, 1156 (1961).

75. Watson, R. E. and Freeman, A. J., Physical Review 123, 521 (1961).

76. Tubis, A., Physical Review 102, 1049 (1956).

77. Bartell, L. S. and Brockway, L. O., Physical Review 90, 833 (1953).

78. Mott, N. F., Proceedings of the Royal Society (London) A127, 658 (1930).

79. Wierl, R., Annalen der Physik 8, 521 (1931).

80. Debye, P., Journal of Chemical Physics 9, 55 (1941).

81. Bartell, L. S., Journal of Chemical Physics 23, 1219 (1955).

82. Bonham, R. A. and Ukaji, T., Journal of Chemical Physics 36, 72 (1962).

83. Schomaker, V. and Glauber, R., Nature 170, 291 (1952).

84. Ibers, J. A. and Hoerni, J. A., Acta Crystallographica 7, 405 (1954).

85. Debye, P., Physikalische Zeitschrift 40, 404 (1939).

86. Morse, P. M., Physical Review 34, 57 (1929).

87. Kuchitsu, K. and Bartell, L. S., Journal of Chemical Physics 35, 1945 (1961).

88. Bartell, L. S., Kuchitsu, K. and de Neui, R. J., Journal of Chemical Physics 35, 1211 (1961).

89. Bartell, L. S. and Brockway, L. O., Review of Scientific Instruments 25, 569 (1954).

90. Bartell, L. S. and Brockway, L. O., Journal of Applied Physics 24, 656 (1956).

91. Bonham, R. A. and Bartell, L. S., Journal of Chemical Physics 31, 702 (1959).

92. Atoji, M., Acta Crystallographica 10, 291 (1956).

93. Bartell, L. S., Kohl, D. A., Carroll, B. L. and Gavin, R. M., Journal of Chemical Physics 42, 3079 (1965).

94. Karle, I. J. and Karle, J., Journal of Chemical Physics 17, 1052 (1949).

95. Degard, C., Bulletin de la Societe Royale des Sciences de Liege 6, 383 (1937).

96. Viervoll, H., Acta Chemica Scandinavica 1, 120 (1947).

97. Bartell, L. S., Brockway, L. O. and Schwendeman, R., Journal of Chemical Physics 23, 1854 (1955).

98. Bartell, L. S. and Brockway, L. O., Journal of Chemical Physics 32, 512 (1960).

99. Boates, T. L. Application of geometric constraints in electron-diffraction studies. Unpublished mimeographed paper. Ann Arbor, Michigan, Department of Chemistry, University of Michigan. 1965.

100. Kimura, M. and Iijima, T., Journal of Chemical Physics 43, 2157 (1965).

101. Bastiansen, O. and Traetteberg, M., Acta Crystallographica 13, 1108 (1960).

102. Morino, Y., Acta Crystallographica 13, 1107 (1960).

103. Morino, Y., Cyvin, S. J., Kuchitsu, K. and Iijima, T., Journal of Chemical Physics 36, 1109 (1962).

104. Bonham, R. A., Journal of Chemical Physics 43, 1933 (1965).

105. Bonham, R. A., Journal of Chemical Physics 43, 1103 (1965).

106. Whittaker, E. T. and Robinson, G. Calculus of observations. 4th ed. New York, New York, D. Van Nostrand Co., Inc. 1952.

107. Schomaker, V., Weinstock, B., Kimura, M. and Smith, D. An electron-diffraction study of WF_6, OsF_6, IrF_6, UF_6, NpF_6, and PuF_6. Unpublished mimeographed paper. Seattle, Washington, Department of Chemistry, University of Washington. 1966.

108. Meisingeth, E., and Cyvin, S. J., Acta Chemica Scandinavica 17, 1805 (1963).

109. Herzberg, G. Molecular spectra and molecular structure. Volume 2. Princeton, New Jersey, D. Van Nostrand Co., Inc. 1945.

110. Badger, R. M., Journal of Chemical Physics 2, 128 (1934).

111. Badger, R. M., Journal of Chemical Physics 3, 710 (1935).

112. Bartell, L. S. and Carroll, B. L., Journal of Chemical Physics 42, 1135 (1965).

113. Rundle, R. E., Journal of the American Chemical Society 85, 112 (1963).

114. Pitzer, K. S., Science 139, 414 (1963).

115. Lohr, L. L. and Lipscomb, W. N. An LCAO-MO study of rare-gas fluorides. In Hyman, Herbert H., editor. Noble-gas compounds. p. 347. Chicago, Illinois, University of Chicago Press. 1963.

116. Gillespie, R. J. and Nyholm, R. S., Quarterly Reviews (London) 11, 339 (1957).

117. Gillespie, R. J., Journal of Chemical Education 40, 295 (1963).

118. Aynsley, E. E. and Hazell, A. C., Chemistry and Industry (London) 1963, 611.

119. Engel, G., Zeitschrift fuer Kristallographie 90, 341 (1935).

120. Brown, I. D., Canadian Journal of Chemistry 42, 2758 (1964).

121. Gillespie, R. J., Canadian Journal of Chemistry 38, 818 (1960).

ACKNOWLEDGEMENTS

I would like to thank Dr. L. S. Bartell for suggesting the problems discussed in this dissertation and for his guidance throughout my studies.

My thanks to Dr. H. B. Thompson for his willingness to discuss research problems and for his helpful advice. I am indebted to Dr. C. L. Chernick for providing the sample of XeF_6 and the auxiliary equipment, and for his invaluable assistance with handling the compound.

I wish to thank Mr. Thomas Boates for providing the computer program for the radial distribution curve analysis and for his advice over the past four years. I would also like to acknowledge the assistance of Mr. Jay Janzen, Mr. Nick Magnani, and Mr. Stan Caldwell on various stages of this research.

I am indebted to the National Science Foundation for financial support for the academic years 1962-63 and 1965-66, and to the Atomic Energy Commision for support for the years 1963-64 and 1964-65.

Special thanks to my wife for her help with the preparation of this dissertation and for her understanding and encouragement during the course of these studies.